Title: Optimization of systemic AAV9 gene therapy in Niemann-Pick disease type C1 mice

Running Title: Systemic AAV9 gene therapy in *Npc1*^{m1N} mice

Summary Blurb: Systemic AAV9-*hNPC1* gene therapy in null *Npc1*^{m1N} mice at higher doses or with earlier administration and treatment of hypomorphic *Npc1*^{I1061T} mice delays disease progression and increases lifespan.

Authors: Avani V. Mylvara[1,2*], Alana L. Gibson[2,3*], Tansy Gu[2,4*], Cristin D. Davidson[1,2+], Art A. Incao[2], Katerina Melnyk[1], Dominick Pierre-Jacques[5], Stephanie M. Cologna[5], Charles P. Venditti[2], Forbes D. Porter[1], William J. Pavan[2]

[1]*Eunice Kennedy Shriver* National Institute of Child Health and Human Development, National Institutes of Health, Department of Human Health and Services, Bethesda, MD; [2]National Human Genome Research Institute, National Institutes of Health, Department of Human Health and Services, Bethesda, MD; [3]Howard Hughes Medical Institute, Department of Cellular and Molecular Medicine, Section of Neurobiology, Division of Biological Sciences, University of California, San Diego, San Diego, CA; [4]University of North Carolina, Chapel Hill, NC; [5]University of Illinois Chicago, Chicago, IL
*Indicates equal contribution

Author Contributions

- AVM – data curation, formal analysis, investigation, methodology, validation, visualization, writing – original draft, writing – reviewing & editing (0000-0002-8741-4008)
- ALG – data curation, formal analysis, investigation, validation, writing – reviewing & editing (0000-0003-2247-7064)
- TG -- data curation, formal analysis, investigation, validation, writing – reviewing & editing (0000-0002-0653-0892)
- CDD – conceptualization, data curation, investigation, project administration, supervision, validation, visualization, writing – original draft, writing – reviewing & editing (0000-0002-5508-8113)
- AAI – investigation, methodology (0000-0001-6801-4562)
- KM – formal analysis, investigation, validation, visualization, and writing- review & editing (0000-0001-9167-5801)
- DP-J – data curation, formal analysis, investigation, methodology, visualization, writing -reviewing & editing (0009-0009-1272-0607)
- SMC – conceptualization, funding acquisition, methodology, project administration, resources, supervision, writing – reviewing & editing (0000-0002-3541-3361)
- CPV – methodology, ideas, writing – reviewing & editing (0000-0001-6599-1253)
- FDP – project administration, supervision, funding acquisition, resources, writing – review & editing (0000-0001-9397-0046)
- WJP – conceptualization, project administration, supervision, funding acquisition, resources (0000-0001-8281-5120)

[+]Corresponding Author (Cristin Davidson)

Abstract (175 words):

Niemann-Pick disease, type C1 (NPC1) is a rare, fatal neurodegenerative disorder caused by pathological variants in *NPC1*, which encodes a lysosomal cholesterol transport protein. There are no FDA approved treatments for this disorder. Both systemic and central nervous system delivery of AAV9-*hNPC1* have shown significant disease amelioration in NPC1 murine models. To assess the impact of dose and window of therapeutic efficacy in $Npc1^{m1N}$ mice, we systemically administered three different doses of AAV9-*hNPC1* at 4 weeks old and the medium dose at pre-, early, and post-symptomatic timepoints. Higher vector doses and treatment earlier in life were associated with enhanced transduction in the nervous system and resulted in significantly increased lifespan. Similar beneficial effects were noted after gene therapy in $Npc1^{I1061T}$ mice, a model that recapitulates a common human hypomorphic variant. Our findings help define dose ranges, treatment ages, and efficacy in severe and hypomorphic models of NPC1 deficiency and suggest that earlier delivery of AAV9-*hNPC1* in a pre-symptomatic disease state is likely to yield optimal outcomes in individuals with NPC1.

Introduction:

Niemann-Pick disease, type C (NPC) is a rare, fatal neurodegenerative disease with an incidence of ~1 in 100,000 live births [1]. This autosomal recessive lysosomal storage disorder is marked by unesterified cholesterol and sphingolipid accumulation in the lysosome, the latter of which is especially prominent in neural tissue. At least 95% of NPC1 individuals have disease associated variants in the integral membrane-bound NPC1 protein located in the lysosome (NPC1 disease, OMIM #257220). The remaining individuals have pathological variants in the NPC2 protein (NPC2 disease, OMIM #607625), a soluble lysosomal protein that transfers unesterified cholesterol to NPC1 [2]. Clinical presentation of both forms of the disease are similar, which is in accordance with previous research demonstrating that NPC1 and NPC2 work together to facilitate egress of cholesterol and likely other lipids from the lysosome [1, 3-6]. Disease severity and onset is highly variable, affecting infants, children, and adults; however, the classical presentation of NPC1 is most often observed in school-age children and typically includes progressive cerebellar ataxia, vertical supranuclear gaze palsy, gelastic cataplexy, motor deficits, cognitive impairment as well as visceral manifestations like hepatosplenomegaly [7, 8]. Miglustat, a glycosphingolipid synthesis inhibitor, is approved for treatment for NPC outside the US and though other potential therapeutics have advanced through trial or to expanded access protocols, none have secured regulatory approval [9-12]. While small molecule therapeutics provide some amelioration, all fail to address the root cause of the disorder – the absence of the NPC1 protein that causes subsequent morbidity and mortality. Gene therapy can provide the replacement of the dysfunctional NPC1 protein to treat the disease [13, 14]. Given the irreversible nature of neurodegeneration and lethality, NPC individuals remain in dire need of effective treatments that a durable gene therapy might provide.

Recent studies have demonstrated that gene therapy, especially those using adeno-associated viral (AAV) vectors, can provide treatments for monogenic and rare diseases. AAVs are already approved for treatment of Spinal Muscular Atrophy (SMA1; onasemnogene abeparvovec-xioi [15]) and RPE65 mutation associated retinal dystrophy (voretigene neparvovec-rzyl [16]) [17-20]. AAV serotypes are well-characterized and increasingly used in clinical trials for monogenic diseases [21-24]. Vectors that use AAV serotype 9, or AAV9, are well documented to cross the blood-brain barrier (BBB) and transduce cells of the central nervous system (CNS) [25-27]. Given the devastating neurological impact of NPC1, a gene therapy targeting the CNS is imperative. Of note, AAV9 also transduces multiple other organ systems, including the liver and peripheral nerves, that are implicated in NPC1 disease [7, 8, 28-30].

We and others have previously demonstrated AAV9 vectors can effectively improve survival and delay NPC1 disease progression in a severe NPC1 murine model ($Npc1^{m1N}$) [21, 31-35]. We will use single

allele notation to indicate homozygosity. Both direct CNS administration (intracerebroventricular or intracisternal magna) [32, 34] and systemic administration (retro-orbital or intracardiac) [21, 31] have successfully ameliorated disease in these mice. Greater success has been noted when using dual routes of CNS administration or administering higher doses of vector to the CNS [34, 35]. Independent studies have demonstrated that ubiquitous promoters provide greater disease correction in *Npc1*^{m1N} mice as compared to neuron-specific promoters [21, 35] and further optimization studies have highlighted the therapeutic potential of novel capsids to improve CNS transduction [33].

While there is a robust foundation for gene therapy studies largely focused on neonatal intervention in severely affected *Npc1*^{m1N} mice, further studies using variable times of delivery and mouse models that recapitulate attenuated forms of the disease have not been fully explored. Nearly all preclinical studies in *Npc1*^{m1N} murine models have targeted neonates [31, 32, 34, 35]. In our previous work [21, 33], AAV9 vectors were administered at pre-symptomatic, weaning age (4 weeks old), but the question has remained of whether late(r) intervention can still be effective following early or post-symptomatic diagnoses in individuals. Previous clinical studies for another rare pediatric genetic disorder, aromatic L-amino acid decarboxylase deficiency, suggest that AAV gene therapy is universally beneficial, but treatment at a younger age was associated with greatest therapeutic effects (NCT01395641, NCT02926066) [36]. Intervention prior to clinical onset of neurologic symptoms in NPC is currently challenging because newborn screening for NPC1 is not yet included on the Recommended Uniform Screening Panel (RUSP) and the average diagnostic delay remains ~4.1 years [37, 38]. Although NPC1 is on the American College of Obstetricians and Gynecologists (ACOG) and American College of Medical Genetics and Genomics (ACMG) suggested carrier screening panel to identify couples at risk for affected pregnancies, it is not routinely screened for. Early intervention prior to neurologic onset might be possible in familial cases and after diagnosis when there is infantile presentation with fetal ascites and liver disease [39-41]. More than 600 pathogenic or likely pathogenic NPC1variants have been described, most of which are missense mutations [42-44]. One of the most prevalent variants results in a missense mutation in the NPC1 p.I1061T protein, causing NPC1 to misfold and undergo endoplasmic reticulum associated degradation (ERAD) [45, 46]. A knock-in, hypomorphic *Npc1*^{I1061T} allele was generated to recapitulate the human disorder [47, 48]: *Npc1*^{I1061T} mice have a slightly protracted disease course compared to the *Npc1*^{m1N} mouse model that has a premature stop codon in the *Npc1* gene resulting in production of truncated, non-functional NPC1 protein [47]. Using *Npc1*^{I1061T} mice, we investigated and confirmed that residual NPC1 protein with compromised stability did not interfere with the efficacy of gene therapy.

Here we build on our previous work, using systemic administration of an AAV9-elongation factor 1α (shortened)-*hNPC1* (AAV9-EF1a(s)-*hNPC1*) vector to treat various mouse models of NPC1 at timepoints later in disease progression. We further examine the therapeutic efficacy of this vector across different doses and in *Npc1*^{I1061T} mice. In aggregate, our results provide foundational preclinical data for the advancement of AAV9-EF1a(s)-*hNPC1* as a disease modulating therapy for individuals with NPC1 deficiency.

Results:

Mice treated with higher doses of AAV9-EF1a(s)-*hNPC1* gene therapy showed increased survival and delayed disease progression.

All mice received a retro-orbital injection of AAV9-EF1a(s)-*hNPC1*, herein referred to as AAV9, and every figure panel following contains the data of 4-28 mice per group (Table S1). To compare the efficacy of AAV9 at varying doses, mice were injected at 4 weeks old (weaning, postnatal day 26-28) with a low, medium, or high dose ($7.87x10^{12}$ vector genomes/kg, $1.28x10^{14}$ vg/kg, or $3.06x10^{14}$ vg/kg, respectively) Based on a Log-Rank, Mantel Cox test of survival with application of Bonferroni's correction, all treated cohorts showed improvement over saline injected mice. Mice treated with high and

medium doses survived longer than low dose and saline-only injected mice (34.6, 21.5, 11.4, and 10.6 weeks median survival, respectively, P<0.0001) (Fig 1A, B). Of note, the low dose injected mice also had improved survival compared to the saline-only group (11.4 vs 10.6 weeks, P=0.0049).

Npc1^{m1N} mice exhibit marked weight loss starting at about 6 weeks old; therefore, the week that mice reached their peak weight and the change in weight from 6 to 9 weeks of age was analyzed. Mice receiving the low dose reached peak weight at 6.9 ± 0.6 weeks, similarly to saline injected controls (6.8 ± 0.7 weeks). Both groups reached peak weight earlier than either medium dose mice (11.3 ± 3.9 weeks) or high dose mice (14.8 ± 3.1 weeks) (Fig 1C, Kruskal-Wallis Test with Dunn's multiple comparisons test). Longitudinal weight data (Fig S1A, B) demonstrates that mice maintain weight and survive longer as the dose of AAV9 increases. Both saline and low dose mice lost weight similarly between 6 and 9 weeks (-14.6% ± 6.8% and -9.0% ± 11.7%, respectively) (Fig 1D). Notably, medium (11.2% ± 13.1%) and high dose (15.3% ± 10.9%) treated mice showed significant differences from both saline and low dose, gaining weight at a similar trajectory to *Npc1*$^{+/+}$ mice (5.6% ± 4.1%) between 6 and 9 weeks of age (One-way ANOVA with Tukey's multiple comparisons test).

To determine the effect of dose on phenotypic progression, five parameters indicative of neurological phenotype (hindlimb clasp, motor function, kyphosis, grooming, and a balance-ledge test) were assessed in the mice at 3-week intervals from weeks 6-18 [49]. Phenotype assessment shows most significant delay of disease onset and progression in high dose mice, but there was still notable delay in medium dose mice. Two-way ANOVA tests with mixed effects analysis were used to estimate how the mean phenotype score changes according to the time of assessment and treatment group. Low dose mice follow the vehicle trajectory of progression (Fig 1E). Between 6 and 9 weeks, all treatment groups were significantly delayed in phenotype onset from vehicle treated, while high dose treated mice were like *Npc1*$^{+/+}$. Between weeks 9 and 12, mice treated with high and medium doses had significantly lower composite scores than low dose and saline injected mice (P<0.0001, two-way ANOVA mixed-effects analysis with Tukey's multiple comparisons test, results presented in Fig S2A). Comparing weeks 15 and 18, high dose treated mice had significantly lower composite scores than medium dose treated (P< 0.01, two-way ANOVA mixed-effects analysis with Tukey's multiple comparisons test), and high dose treated mice were not significantly different from *Npc1*$^{+/+}$ but still trended upwards.

Higher doses of AAV9 result in greater viral transduction in *Npc1*^{m1N} mice.

To evaluate the efficacy of vector transduction in various tissues, droplet digital PCR (ddPCR) was performed using cerebrum (Fig 2Ai, ii, 2C) and liver (Fig 2Bi, ii) to determine *hNPC1* copy number at 10 weeks of age or the humane endpoint/survival. At 10 weeks old, the typical age for humane endpoint without therapeutic intervention in our colony, there were higher copy numbers in the high dose cerebrum compared to all other treatment groups (Fig 2Ai). There was only a significant predictive relationship between *hNPC1* copy number and lifespan in the cerebrum within the medium dose group (Fig 2Aii), but there was a strong correlation between copy number in cerebrum and increased survival when all treated mice are grouped compared to saline-injected mutants (Fig 2C). Of note, two mice had exceptionally and unexpectedly high CNV in the cerebrum in the medium dose treated group, and seem to drive a significant relationship between CNV and lifespan within the medium dose group, but not when all treated mice are grouped together (Fig 2Aii, C). In the liver, there were higher copy numbers in the high dose mice compared to other treatment groups at 10 weeks (Fig 2Bi), but there was no predictive relationship between copy number and increased survival within each treatment group (Fig 2Bii). Additional analysis of 10-week-old mice was performed to understand copy number variation across different organs (spleen, kidney, lung, muscle, cerebellum, brain stem). Overall, an increased dose (particularly high dose) of gene therapy led to greater copy numbers (Fig 2D).

Western blots were performed to determine the level of NPC1 protein present in brain and liver tissue in 10-week old *Npc1*^{m1N} mice where the only protein present would be a result of vector transduction (Fig 2C, F, & representative blot Fig S5). NPC1 levels assessed in the cerebrum did not reveal significant levels of protein for any of the doses, though cerebrum from high dose treated mice revealed very low, albeit detectable levels of protein (Fig 2C). In livers, NPC1 protein was present in medium and high dose treated mice. High dose treated mice displayed a greater level of NPC1 protein compared to *Npc1*$^{+/+}$ (not considered significant). Low dose treated mice did not have appreciable levels of detectable protein (Fig 2F).

Higher doses reduce pathology in the brain and liver and preserve cerebellar Purkinje neurons of 10-week-old mice.

Immunofluorescent staining of the brain and immunohistochemical staining of the liver was performed to assess cholesterol storage in the cerebellum, health of the cerebellum, and inflammation in age-matched 10-week-old mice. Parallel assessments of GFAP (astrocytes), calbindin D (Purkinje neurons), and CD68 (microglia) and NPC1 proteins via western blot were used for quantification. Unesterified cholesterol storage, as ascertained by filipin labeling, appears modestly reduced with high dose gene therapy when compared to lower doses or saline in 10-week-old *Npc1*^{m1N} mice (Fig 3A). Neuroinflammation as indicated by GFAP labeling of astrocytes and western blot of cerebellum is reduced (not statistically significant) with increasing dose and appears to correlate with higher copy numbers of *hNPC1* (Fig 3A, C, & representative blot Fig S6). Purkinje neuron survival appears to increase in the cerebellum as gene therapy dose increases but protein levels in treated mice are significantly less than in *Npc1*$^{+/+}$ mice; Purkinje neuron preservation seems to be correlated with copy number of *hNPC1* (Fig 3A, D, representative blot Fig S7). Anterior to posterior loss of Purkinje neurons is concurrent with previous findings in NPC1 transcriptomics of the cerebellum (Fig 3A; [50]). Higher CNV also correlates with reduced neuroinflammation, as evidenced by decreased immunostaining of microglia in posterior lobules of the cerebellum and apparent reduced CD68 protein levels in the cerebellum of high dose mice (Fig 3B, E respectively, representative blot Fig S6).

In the cerebellum, ddPCR of the *hNPC1* gene (Fig 3F) reveals an apparent linear relationship between increasing copy number and survival in medium dose mice, though it is not significant in any other treatment group. There are two outliers in the medium dose mice (same two mice as seen in the cerebrum analysis) that when removed, mean the relationship between CNV and survival in this group is not significant. NPC1 levels were assessed in the cerebellum via western blot, demonstrating higher apparent levels of NPC1 as dose increased (Fig 3G, representative blot Fig S7).

NPC1 liver pathology includes an increased presence of myeloid cells (CD68+) due to increased lipid storage burden within these cells, many of which are macrophages like Kupffer cells (KC) (Fig 4A, B). Lipid laden myeloid cells are highly abundant in *Npc1*^{m1N} mice administered saline or low dose gene therapy. There is a dose-dependent effect on myeloid cell labeling, with percent CD68+ immunohistochemical labeling decreasing with more effective, higher doses (Fig 4B, C). Fluorescent imaging also reveals decreases in cholesterol storage at high doses, demonstrated by diminished presence of myeloid cells (CD68) and a decrease in amount of filipin labeling (Fig 4A; specifically, inset for high dose liver with arrows indicating groups of cells without cholesterol storage). Overall, increased doses appear to reduce liver pathology.

Upon evaluation of the survival, weight curves, and phenotype data from the three main studies (dose, age at treatment and hypomorphic model), we observed the greatest disease amelioration with a high dose; thus, we carried out more detailed analysis and quantification of pathology in the dose cohorts. Age of

treatment and efficacy in the *Npc1*^{I1061T} model data followed similar trends with respect to correlation between survival time and impact on pathology.

Alterations in sphingolipid distribution following gene therapy administration.

In addition to cholesterol accumulation, multiple other lipid classes exhibit altered levels resulting from impaired NPC1 protein function [51, 52]. Mass spectrometry imaging was performed to evaluate the effect of gene therapy on lipid distribution following administration. A stark contrast in distribution was observed when comparing mutant and *Npc1*$^{+/+}$ mice, especially within the sphingolipid class (Figure S8). Gangliosides such as GM2 are known to accumulate within the brain in *Npc1*^{m1N} mice [53]. *Npc1*$^{+/+}$ mice demonstrated little to no ganglioside accumulation within the brain, compared to the mutant mice which displayed high ganglioside accumulation, primarily in the frontal cortex and lobule X in the cerebellum. With increasing doses of gene therapy, a corresponding qualitative reduction in ganglioside accumulation was observed in both the cortex and cerebellum (Figure S8A). In contrast, the sphingolipid hexosylceramide (HexCer 46:4;O3) is increased in the cerebellum of *Npc1*$^{+/+}$ mice compared to the mutant. While the frontal cortex remains largely unchanged between doses, a change in lipid abundance is observed at differing AAV9 doses (Figure S8B). While hexosylceramide signal increased throughout the cerebellum, the rostral lobes of the cerebellum (lobules I-V) display a higher abundance compared to the rest of the cerebellum. Another sphingolipid, dihydroceramide (Cer 32:2;O3), was found to be increased in mutant mice compared to *Npc1*$^{+/+}$ mice. However, reduction in dihydroceramide accumulation is less apparent, though high and medium dose gene therapy do appear to impact this lipid (Figure S8C).

Treating mice at 4 weeks of age with AAV9-EF1a(s)-*hNPC1* gene therapy significantly improves survival and reduces disease progression compared to treatment at 6 or 8 weeks of age.

Npc1^{m1N} mice were treated with 1.28x10^{14} gene copies/kg of AAV9-EF1a(s)-*hNPC1* at 4 weeks (pre-symptomatic), 6 weeks (early-symptomatic), or 8 weeks (late-symptomatic) to determine the therapeutic window of efficacy for gene therapy. Comparison of survival between these groups (Fig 5A) shows that mice injected at 4 weeks had a significantly longer median survival (21.5 weeks) than saline injected mice (10.6 weeks) or mice treated at either 8 weeks (11.9 weeks) or 6 weeks (13.2 weeks). Bonferroni's correction factor was applied for 6 comparisons that lowered level of significance to P=0.0083 for this Log-rank Mantel Cox survival test (Fig 5B).

Week of peak weight and percent weight change between 6 and 9 weeks was also assessed to determine how gene therapy affected weight. Mice injected at 4 weeks old had a significantly later week of peak weight (11.3 ± 3.9 weeks) than saline injected mice or mice treated at 6 or 8 weeks of age (P <0.0001) (Fig 5C). Mice treated at 6 and 8 weeks were not different from each other (6.8 ± 2.3 weeks, 6.7 ± 0.6 weeks respectively) nor from saline injected mice (6.8 ± 0.7 weeks) (One-way ANOVA with Tukey's multiple comparisons test). Only mice injected at 4 weeks and *Npc1*$^{+/+}$ mice gained weight from 6-9 weeks (11.2% ± 13.1%, 6.0% ± 4.1% respectively), and only mice injected at 4 weeks were significantly different from all other groups except *Npc1*$^{+/+}$. *Npc1*^{m1N} mice injected at 6 or 8 weeks of age lost weight similar to saline injected *Npc1*^{m1N} mice (-12.2% ± 7.7%, -20.0% ± 10.9%, and -14.6% ± 6.8%, respectively) (Fig 5D, Ordinary one-way ANOVA with Tukey's multiple comparisons test). Longitudinal weight data further supports that in both male and female cohorts, mice treated earlier maintained weight and survived longer (Fig S2C, D).

Evaluating disease progression via the composite phenotype assessment demonstrated benefit early in the disease course for the group injected at 4 weeks old. Between 6 and 9 weeks of age, mice injected pre-symptomatically (4 weeks old) had significantly lower phenotype scores than the other two treatment groups. From 9-12 weeks, all treated groups progressed at a slower rate than saline injected mice, and mice injected at 4 weeks maintained significantly lower scores than all other groups apart from *Npc1*$^{+/+}$

and lived longer (Fig 5E) (two-way ANOVA mixed effects model with Tukey's multiple comparisons test, results presented in Fig S2B).

Earlier treatment leads to greater transduction efficiency and reduces cerebellar pathology.

Further analyses were performed to determine the differential transduction efficiency of the same vector at different ages of injection. ddPCR was used to measure *hNPC1* copy number in the cerebrum and liver. In the cerebrum, for both 4- and 6-week-old treated mice, higher copy numbers predicted longer lifespans suggesting transduction in the brain aids in lengthening lifespan as shown by linear regression (Fig 6A). Copy number in the brain did not predict lifespan in mice treated at 8 weeks old. Of note, in the 4-week-old treated mice, there are two outliers (same from medium-dose group) that do not drive significance. For further corroboration, copy number was also evaluated across all groups at an age-matched time point of 9 weeks (late-stage disease, shortly before humane endpoint). At this time point, mice injected post-symptomatically (8 weeks old) had the highest copy number in the cerebrum and were significantly different than saline injected and other treated groups (Fig 6B).

In the brain, immunofluorescent imaging was used to assess neuroinflammation and Purkinje neuron survival in 9-week-old, age-matched mice. When assessing overall loss of Purkinje neuron survival and particularly in anterior lobules of the cerebellum, treatment with AAV9 at 4 weeks, as compared to saline-injected mice and mice treated at 6 or 8 weeks, appears to delay Purkinje neuron loss (Fig 6C). Similarly, it appears that early treatment at 4 weeks reduces neuroinflammation in posterior lobules of the cerebellum, as demonstrated by reduced IBA1 staining when compared to saline-injected mice and mice treated at later time points (Fig 6D).

In the liver, higher copy numbers predicted increased lifespan in only 6-week-old treated mice; all other relationships between copy number and age were not predictive in liver (Fig S3A). At 9 weeks of age, mice treated at 8 weeks again had higher *hNPC1* copy numbers than other treated mice and saline-injected mice (Fig S3B). At the same age, myeloid cell pathology in showing liver lipid storage burden reveals reduced CD68+ area in 6-week-old treated mice compared to mice treated at 4 weeks and saline-injected mice (Fig S3C, D).

AAV9-EF1a(s)-*hNPC1* improved lifespan, delayed disease progression, and decreased liver pathology in *Npc1*^{I1061T} mice.

To evaluate whether AAV9-EF1a(s)-*hNPC1* was effective in a hypomorphic mouse model of NPC1 disease, *Npc1*^{I1061T} mice were treated with $1.28x10^{14}$ gene copies/kg of AAV9-EF1a(s)-*hNPC1* at 4 weeks old. Survival of treated mice was compared to survival of saline-injected mice (Fig 7A). AAV9 treated mice lived to a median age of 22.0 weeks which was significantly longer than 15.0 weeks for saline-injected mice (Log-rank Mantel-Cox test, $P<0.001$). Of note, *Npc1*^{I1061T} mice live to a median survival of about 17.9 weeks, whereas *Npc1*^{m1N} mice have a median survival of about 10.5 weeks [47].

To evaluate AAV9 efficacy in slowing a common marker of NPC1 progression, weight loss, week of peak weight and percent weight change from 10 to 14 weeks was measured (adjusted from null model based on lifespan of *Npc1*^{I1061T} model). Treated mice appear to reach peak weight later than saline-injected mice, but were not significantly different (12.9 ± 3.8 weeks vs. 10.9 ± 1.1 weeks, Wilcoxon matched pairs signed rank test) (Fig 7B). Treated mice gained weight from 10-14 weeks (3.8% ± 6.0%), similar to *Npc1*$^{+/+}$ mice (7.3% ± 2.7%) (Kruskal-Wallis test with Dunn's multiple comparisons test, $P=0.02$). In contrast, saline injected mice lost weight (-12.3% ± 11.0%) and were significantly different from treated ($P<0.05$) and *Npc1*$^{+/+}$ ($P<0.0001$) (Fig 7D).

Disease phenotype was also evaluated in treated and untreated mice to determine efficacy of gene therapy in slowing progression. Mice were evaluated on the same metrics as previously described where higher composite scores indicate worsening disease severity. From weeks 9-15, AAV9 treated *Npc1*^{I1061T} mice had significantly lower composite scores compared to saline-injected mice (9 weeks: P=0.03; 12-15 weeks: P<0.0001; two-way ANOVA with Tukey's multiple comparisons test), though were still significantly higher than *Npc1*$^{+/+}$ from 9-15 weeks (P<0.0001, Fig 7D).

To determine the ability of the AAV9 to transduce cells, ddPCR was used to measure *hNPC1* copy number in the cerebrum and liver. In both tissues, there were significant relationships between *hNPC1* copy number and age of humane endpoint; however, the relationship was positive in the cerebrum, and negative in the liver (Fig S4 A, C). At 14 weeks, the typical end stage for untreated mice, copies of *hNPC1* in both the cerebrum and liver were present, like values observed in treated *Npc1*^{m1N} mice (Fig S4 B, D, Fig 2 A, E).

To further analyze therapeutic efficacy, liver lipid storage burden was assessed with immunohistochemical staining of myeloid cells in age-matched 14-week-old mice. *Npc1*^{I1061T} mice show myeloid cell enlargement due to cholesterol accumulation unlike normal livers from *Npc1*$^{+/+}$ mice. Treated mice show partial reduction of myeloid cell enlargement compared to saline-injected mice (Fig S4E, F) suggesting gene therapy is effective in reducing cholesterol accumulation in the liver, albeit not to normal *Npc1*$^{+/+}$ levels.

Discussion

Here, we detail a highly effective AAV9 gene therapy that can be delivered systemically, over a range of doses and times in the *Npc1*^{m1N} model of NPC1 deficiency. Administration of higher doses of AAV9, especially in the pre-symptomatic period, significantly increased survival, slowed weight loss, and lessened disease severity compared to mice receiving lower vector doses or when treated later in life. Additionally, we define the durability of AAV9-EF1a(s)-*hNPC1* using knock-in *Npc1*^{I1061T} mouse model as evidenced by increasing lifespan and ameliorating disease progression.

We examined dose, age at intervention, and type of genetic variation (null vs missense mutation) as key factors for optimization of systemically delivered AAV9-hNPC1. Previous studies have established systemic and CNS routes of administration of gene therapy for NPC disease to be effective, and notably that higher doses of vector delivered intracerebroventricular (ICV) improved neurological and motor symptoms of *Npc1*^{m1N} mice when compared to lower doses [21, 31-35]. These studies, however, did not look at varying doses when injected systemically at a juvenile time point. In accordance, we show higher doses of AAV9 injected retro-orbitally improved disease progression as demonstrated by significantly longer lifespans, lower phenotype scores, weight maintenance, and reduced pathology when compared to lower doses.

Some proof-of-concept NPC1 gene therapy preclinical studies have been conducted in neonatal *Npc1*^{m1N} mice. While many NPC1 individuals are severe and present early in life, even in utero, others have varying ages of onset. Many exhibit the first neurological sign in their childhood/juvenile years followed by significant diagnostic delay, and NPC1 is not on the RUSP or on the carrier screening panel; therefore, we sought to assess therapeutic efficacy of AAV9-EF1a(s)-*hNPC1* in early and post-symptomatic disease states. We show that survival is correlated with cerebral *hNPC1* gene copy number following earlier intervention, highlighting the importance of early treatment to ameliorate disease progression. Moreover, *Npc1*^{m1N} mice treated at 4 weeks of age, as compared to those treated at 6 or 8 weeks, demonstrate significant weight gain during disease course and most importantly, survive longer. Of note, the *Npc1*^{m1N}

mice treated at 6 weeks do show slight benefit from AAV9 treatment, namely modest increase in survival when compared to mice treated at 8 weeks or saline-injected mice, suggesting that improvements can still occur when gene therapy is provided at an early symptomatic time point.

The *Npc1*^{I1061T} model has not been previously investigated. Consistent with the null model, our data shows a significant increase in survival, delay of weight loss, improvement in phenotype, and reduction of pathology following systemic administration of AAV9-EF1a(s)-*hNPC1*. Importantly, *Npc1*^{I1061T} mice are more representative of corresponding human condition as NPC1 p.I1061T encodes a misfolded protein targeted for ERAD [47, 48]. The success of treatment in both mouse models highlights the immediate translational potential of this vector, and presents opportunities for further investigation, including examination of other routes of delivery, ages of administration, efficacy in larger animal models, and even combination with other therapeutic agents to potentially increase efficacy. Importantly, several clinical trials using peripherally administered gene therapy for neurological diseases are well underway (SMA1 NCT03461289, NCT03306277, and [17]; MPSIII: NCT02716246, NCT03315182; Canavan: NCT04498396).

In aggregate, our studies demonstrate that systemic delivery of AAV9-EF1a(s)-*hNPC1* can have significant impact on NPC1 disease phenotype and improve survival in severe and milder mouse models of the disorder. In addition to mitigation of CNS disease, our data suggests correction in the liver can be achieved with AAV9-EF1a(s)-*hNPC1*, as evidenced by hepatic transgene expression and reduced liver pathology in the treated mice. Given the great success using peripherally administered AAV9 gene therapy to treat SMA1, and the extension to a wide range of other neurological disorders, including MPSIII and Canavan disease, the preclinical enabling studies presented here should serve to facilitate the clinical translation of a promising new therapy for individuals with NPC1 deficiency.

Materials & Methods

Vector construction and production

The vector, AAV9-EF1a(s)-*hNPC1* was previously described and produced by the University of Pennsylvania Vector Core [21].

Animals

All animal work in these studies was carried out in accordance with the National Institutes of Health Animal Care and Use Committee approved protocols. Heterozygous (BALB/cNctr-*Npc1*^{m1N}/J strain; Jackson Laboratory strain # 003092) *Npc1*$^{+/m1N}$ mice were crossed to obtain homozygous mutants (*Npc1*$^{m1N/m1N}$) and wildtype controls (*Npc1*$^{+/+}$). *Npc1*^{I1061T} mice were generated by crossing heterozygous *Npc1*$^{+/I1061T}$ mice (B6.129-*Npc1*^{tm1Dso}/J strain; Jackson Laboratory strain # 027704) to obtain homozygous mutants and *Npc1*$^{+/+}$ controls. We will use single allele notation to indicate homozygosity. Mice were weighed weekly and then more frequently as the disease progression neared humane endpoint. Mice were euthanized at a predefined humane endpoint which occurred when two of the following four criteria were met: weight falling below 70% of peak weight, repeatedly falling to side during movement, dull eyes or palpebral closure of eyes, or reluctance to move.

As per the ARRIVE Essential 10, the following information refers to the studies contained herein. All studies included vehicle or untreated mice (mutant or wildtype, respectively) as control groups. The same control mice from the *Npc1*^{m1N} line were used for the dose and age at injection studies while the appropriate groups of control mice from the *Npc1*^{I1061T} line were used for the corresponding study. A total of 238 mice were used in these studies. Group sample size is stated in the legend or figure for each analysis. Data for dose and age of treatment study includes all saline and medium dose AAV9 injected *Npc1*^{m1N} mice as well as untreated *Npc1*$^{+/+}$ at 4 weeks. No specific exclusion criteria were set a priori, and

all mice included in the studies were randomly assigned to treatment or control groups using a blocking method. Except for the researcher overseeing the studies, those involved in gene therapy administration and data acquisition remained blinded to the greatest extent possible. Evaluators were always blinded to treatment and genotype when performing the phenotype assessment. The primary outcome measure was survival. Secondary outcome measures included behavioral assessments, weight, gene copy number, and pathology. Details of statistical analyses are found in either the methods or figure legends. Experimental animals, procedures, and results are contained with the methods and results of this publication.

Phenotypic Assessment

Mice were tested starting at 6 weeks of age and every three weeks thereafter until humane endpoint or inability to complete the evaluation. The phenotype score evaluates five behaviors associated with the NPC1 phenotype in diseased mice as previously described: hindlimb clasp, motor function, kyphosis, grooming, and a balance-ledge test for cerebellar ataxia [49]. Each phenotype is scored from 0 to 3 with increasing scores representing a more compromised disease state.

Phenotypic testing was carried out in a blinded fashion such that individual mice within a cage had distinct tail markings. Evaluators had access only to cage card numbers and tail markings to identify mice. The order in which mice were tested varied for each testing date. All animals were group housed.

Administration of vector

Treated *Npc1*^{m1N} mice received a retro-orbital injection of AAV9-EF1a(s)-*hNPC1* at 4 weeks (weaning), 6 weeks, or 8 weeks of age. *Npc1*^{I1061T} mice received a retro-orbital injection of AAV9-EF1a(s)-*hNPC1* at 4 weeks old. Control littermate *Npc1*^{m1N} or *Npc1*^{I1061T} received a retro-orbital injection of 0.9% saline at 4 weeks or the specified age. Mice were anesthetized using isoflurane for 30-60s and then injected retro-orbitally with a 30-gauge needle affixed to a 0.3 cc syringe. The study compared *Npc1*^{m1N} mice administered vehicle (saline) or gene therapy vector (AAV9-EF1a(s)-*hNPC1*) at different ages and different doses. Some control *Npc1*$^{+/+}$ mice received retro-orbital injections of saline while others remained un-injected.

Across cohorts, mice at 4 weeks were given a dose of $1.2x10^{12}$ gene copies/mouse, which was an average of $1.28x10^{14}$ vector genomes/kg (vg/kg, medium dose). For the age at injection study, the weight at injection was used to calculate the volume necessary to deliver $1.28x10^{14}$ vg/kg for each mouse and subsequently administered at either 6 or 8 weeks of age. For the dosage study, the low dose was $7.87x10^{12}$ vg/kg and the high dose was $3.06x10^{14}$ vg/kg (maximum dose allowed by vector concentration).

Tissue collection and homogenization

Mice were anesthetized with an intraperitoneal injection of Avertin (lethal dose of 0.04 mL/gm) for euthanasia as previously described [33]. When mice were insensate, the chest cavity was opened, and mice were perfused with 0.9% saline. Immediately, half of the brain, one lobe of the liver, and a piece of spleen, kidney, lung, and leg muscle were collected and frozen on dry ice for tissue homogenization. Mice were then perfused again with 4% paraformaldehyde to fix tissues; remaining organs (half of the brain, liver) were collected and stored post-fixation in 4% PFA overnight and then rinsed and stored in PBS.

A Benchmark Scientific Beadbug homogenizer was used to homogenize frozen tissue with UltraPure water. Tissue was placed in tubes with 3 mm zirconium beads (cerebrum, cerebellum, brainstem, liver, spleen, leg muscle) or 1.5 mm zirconium beads (kidney, lung) and homogenized 3 times for 30 seconds at speed 400. Resulting homogenate was aliquoted into tubes for DNA extraction and protein analysis, the latter of which also had RIPA buffer with proteinase inhibitor cocktail (11 836 170 001; Millipore Sigma, Burlington, MA) [33].

Western blotting

Protein levels from cerebrum, cerebellum, and liver homogenates were quantified using a BCA Assay (23225, Thermo Fisher Scientific, Waltham, MA). Equal amounts of protein (50 ug for liver, cerebellum, and cerebrum) were run on 4-12% Bis-Tris SDS-polyacrylamide gels (NP0321BOX/Invitrogen by Thermo Fisher Scientific) and separation was achieved via electrophoresis; protein was then transferred to a nitrocellulose membrane (Life Technologies) and blocked for 1 hour in 0.01% PBSTween and 5% BSA. Samples were incubated for 1 hour at room temperature on a rocker with primary antibody (Table S2). Secondary antibodies were incubated for 1 hour at room temperature (Table S2). Imaging of bands was done with the LI-CORE Odyssey Imaging System.

Histology

Brain and liver tissue from each group were acquired at 9 or 10 weeks of age (*Npc1*^{m1N}), 14 weeks of age (*Npc1*^{I1061T}), or humane endpoint (both models). Post-fixation tissues were embedded in agarose blocks (3.5% agarose, 8% sucrose, phosphate buffered saline - PBS) and sectioned parasagittaly (30 µm) using a Leica VT1200 S vibratome. Free-floating sections were collected, incubated in 1.6% H_2O_2 in PBS, then washed in 0.25% Triton X-100/PBS (PBSt). After blocking for 1 hour at room temperature in PBSt/normal goat serum, samples were incubated in primary antibodies overnight at 4°C (Table S2). Samples were washed in PBSt and then incubated with secondary antibodies for 30 minutes at 37°C (AlexaFluor 488 or 594; Table S2). Filipin staining (Sigma-Aldrich, F9765) was finally performed to allow visualization of unesterified cholesterol accumulation (0.05mg/mL) with a 20-minute incubation. ProLong Gold mounting medium alone (Thermo Fisher Scientific, P36934) or with DAPI (Thermo Fisher Scientific, P36935) was used to coverslip after mounting slides.

For immunohistochemical staining after primary antibody incubation, slides were incubated in biotinylated secondary antibody and washed in PBSt. A biotinylated horse radish peroxidase (HRP) was preincubated with avidin to form Avidin-Biotin Complex (ABC; Vector Laboratories SK-4100) and the tissues were incubated in ABC (in PBS) for 1 hour. Tissues were then washed in PBS and incubated for 10 minutes in a 3,3'-Diaminobenzidine (DAB; Vector Laboratories PK-4000) solution before mounting and cover slipping with VectaMount (Vector Laboratories, H-5700).

Histoserv, Inc. (Germantown, MD) performed paraffin embedding (FFPE tissues). For immunofluorescent staining, FFPE sections (3 um) were collected and underwent antigen retrieval in a citrate (pH 6.0, Electron Microscopy Sciences, 62706-10) or Tris-EDTA (pH 9.0, Abcam, AB93684) buffer. Slides were then incubated in primary antibody diluted in antibody diluent with BSA and preservative (Thermo Fisher Scientific, 003218) at 37°C for 1 hour, washed in PBS, and incubated in secondary antibodies for 30 minutes at 37°C (Table S2). Tissues were then coverslipped with ProLong Gold mounting medium with or without DAPI.

Image capture and analysis

Fluorescent imaging was performed with an inverted Zeiss AxioScan Z1slide scanner with Zen Blue 3.8 as previously described in [33]. Brightfield images were captured on the same Zeiss AxioScan Z1 slide scanner. Adobe Photoshop 2023 (v.23.5.0) and 2024 (v.25.1.0) was used to modify all images in a figure/group identically by resizing and adjusting brightness and/or contrast.

Quantification of CD68 area

Percent of positive CD68 area relative to total area in liver sections was determined according to methods previously described [54] using Image-Pro. V11 software (Media Cybernetics, Inc.). Images were processed using ten regions of interest with total area 900,000 µm^2 to determine average percent positive area.

Copy number analysis by ddPCR

Vector copy number was measured by droplet digital PCR (ddPCR) as previously described with NPC1 and GAPDH primers (Bio-Rad; [33]). 0.5-50 ng of DNA was used for gene copy number quantification with brain (cerebrum, cerebellum, or brainstem) and liver homogenates. Additional organs including spleen, kidney, lung, and leg muscle were assayed for the 10-week-old cohort in the dose study, using 0.5-5 ng of DNA per reaction. Signals for droplets were either positive or negative for hNPC1 and/or GAPDH as determined using BioRad's QuantaSoft version 1.7.4.0917 software.

Mass spectrometry imaging and lipidomics

The fresh frozen half of the brain was sectioned on a CryoStar NX50 Cryostat set to -12°C in preparation for mass spectrometry imaging. The frozen tissue was divided into 10 µm thick sections, which were then promptly thaw-mounted onto ITO slides (MIDSCI) and stored at -80°C. Immediately prior to imaging sections, the slides were removed from the -80°C freezer and washed with ice cold 50 mM ammonium formate for 20 seconds then dried in vacuo. 9-aminoacridine and 2,5-dihydroxybenzoic acid were chosen as the matrices for negative and positive mode respectively. One hundred milligrams of solid matrix was dissolved in 10 mL of 50:50 H_2O:ACN + 0.2% TFA and filtered using a 0.2 µm syringe filter. Filtered matrix was applied to the slide using the HTX TM Sprayer.

Mass spectrometry imaging was performed on a Bruker RapifleX MALDI TOF with a 10 kHz laser set to 60% power, 500 laser shots per pixel, and a step size of 35 µm. The instrument was operated in negative and positive mode within an m/z range of 200-1800. All data processing including region-of-interest determination, spatial segmentation, mass spectra extraction and image generation were performed using Bruker's FlexImaging software. LIPID MAPS and the Human Metabolome Database were used to annotate and identify lipids according to accurate mass measurements.

Statistical analysis

Randomization was achieved with multiple cohorts. Mice within each cohort were included from each age at injection group or at each dosage. Statistical analysis was performed using GraphPad Prism version 9.5.1 for Windows or Mac. Normality was evaluated for data sets and appropriate parametric or nonparametric tests were selected for further analysis. Data is presented as mean ± SD. Kaplan Meier survival curves used Log-Rank Mantel-Cox test to assess significance, with a Bonferroni-correction applied for $P<0.0083$ for multiple (six) comparisons. Other statistical tests were as follows: Kruskal-Wallis test with Dunn's multiple comparison's test, one-way ANOVA with Tukey's multiple comparisons test, two-way ANOVA with Tukey's multiple comparisons test, linear regression test (all multiple comparisons test use post hoc Bonferroni's correction). In all figures: * $P<0.05$, ** $P<0.01$, *** $P<0.001$, **** $P<0.0001$.

Acknowledgments:

We thank Laura L. Baxter for her support and instruction in statistical analysis as well as Stephen Wincovitch for imaging and quantification support. We are grateful for the technical assistance in digital droplet PCR provided by the National Cancer Institute Genomics Core. We sincerely acknowledge the NIH animal care and veterinary staff for the care of mice used in these studies. We also recognize the driving force behind this work: individuals with NPC1 disease. Their perseverance in the face of this debilitating disease inspires and humbles us.

Funding

This work was supported by the Intramural Research Program of the National Human Genome Research Institute (NHGRI) at the NIH (1ZIAHG000068-16), the *Eunice Kennedy Schriver* National Institute of Child Health and Human Development (NICHD) at the NIH (ZIAHD008988), grants from the NIH

(R01NS114413, R01NS124784), and the Ara Parseghian Medical Research Fund at the University of Notre Dame. AVM, ALG, TG, AI, CPV, and WJP were supported by the Intramural Research Program at NHGRI; CDD, KM, FDP were supported by the Intramural Research Program at NICHD. Additional support for CDD came from the Support Of Accelerated Research for NPC (Hide & Seek Foundation and Dana's Angels Research Trust). DP-J was supported by the Bridge to Doctoral Program and the Diversifying Faculty in Illinois Fellowship.

Conflict of Interest Statement

CPV and WJP have NIH patents filed on work related to NPC1 genes and the AAV gene therapy treatment of NPC1 (US Patent Publication Numbers 20180104289, 20210113635).

Figure 1: *Npc1*^{m1N} mice treated with AAV9-EF1a(s)-*hNPC1* vector show increased survival and delayed disease phenotype progression.
(A) Kaplan-Meier survival curve of mice treated with low, medium, and high dose AAV9 and saline injected mice. **(B)** Table of median survival for each treatment group, significance (Mantel-Cox log rank test) of data from (A). Level of significance is P<0.0083 based on Bonferroni's correction with 6 comparisons. **(C)** Week at which mice reached peak weight (Kruskal-Wallis with Dunn's multiple comparisons test). **(D)** Percent weight change between 6 and 9 weeks old (One-way ANOVA with Tukey's multiple comparisons test). For (C, D): saline n =15, low dose n = 10, medium dose n = 24, high dose n = 8; for (D): *Npc1*$^{+/+}$ n = 21. **(E)** Composite phenotype scores for each dosage group with measurements taken every 3 weeks, starting at 6 weeks. Higher scores indicate disease progression (results presented in Fig S2A) (saline n = 14, low n = 10, medium n = 13, high n = 8, *Npc1*$^{+/+}$ n = 21). For all: * P<0.05, ** P<0.01, *** P<0.001, **** P<0.0001. Data presented as mean ± SD for C, D, E.

Figure 2: Efficacy of viral transduction in cerebrum and liver varies depends on dose of AAV9.
(A,B) Analysis of *hNPC1* copy number in the cerebrum (A) and liver (B). **(Ai, Bi)** Copy number of *hNPC1* in cerebrum (Ai) and liver (Bi) from 10-week-old mice (One-way ANOVA with Tukey's multiple comparisons test). For Ai, Bi, C: (saline n = 6, low n = 5, medium n = 6, high n = 6, *Npc1*$^{+/+}$ n = 9). **(Aii, Bii)** Linear regression of *hNPC1* copy number in the cerebrum (Aii) and liver (Bii) in end stage mice. For Aii (saline n = 14, low n = 9, medium n = 20, high n = 6, *Npc1*$^{+/+}$ n = 17). For Bii (saline n = 14, low n = 9, medium n = 18, high n = 5, *Npc1*$^{+/+}$ n = 17). **(Aiii, Biii)** NPC1 protein levels were assessed via western blot in 10-week-old mice to confirm amount of NPC1 protein in the cerebrum (Aiii) and liver (Biii). For Aiii, Biii (One-way ANOVA with Tukey's multiple comparisons test) (saline n =6, low n = 5, medium n = 6, high n = 6, *Npc1*$^{+/+}$ n = 7). **(C)** Linear regression of copy number in cerebrum across all treated groups with lifespan (saline n = 14, treated n = 35, *Npc1*$^{+/+}$ n = 17). **(D)** Gene copy numbers were measured for various organs at 10 weeks old. For all: * P<0.05, ** P<0.01, *** P<0.001, **** P<0.0001. Data presented as mean ± SD for Ai, Bi, Aiii, Biii, D.

Figure 3: Amelioration of pathology is dose dependent for AAV treated mice at 10 weeks old.
(A) Unesterified cholesterol storage marked by filipin labeling in anterior lobules (lobule IV/V) of the cerebellum (top row). Astrocytes marked by GFAP labeling (middle row). Purkinje neurons are visualized by Calbindin D labeling (bottom row) (free floating sections). **(B)** Microgliosis as evidenced by IBA1 immunostaining in posterior lobules (lobule IX) of the cerebellum (formalin-fixed, paraffin embedded sections). For (A, B) Scale bar = 1000 microns for panels and 250 microns for sagittal cerebellar section. **(C, D, E, G)** Protein levels for GFAP (C), Calbindin (D), CD68 (E), NPC1 (G) were assessed via western blot for each 10-week-old mice cohort (One-way ANOVA with Tukey's multiple comparisons test) (saline n = 6, low n = 5, medium n = 6, high n = 6, *Npc1*$^{+/+}$ n = 8). **(F)** Linear regression of *hNPC1* in cerebellum and survival of mice (saline n = 14, low n = 9, medium n = 20, high n = 6, *Npc1*$^{+/+}$ n = 17). For all: * P<0.05, ** P<0.01, *** P<0.001, **** P<0.0001. Data presented as mean ± SD for C, D, E, G.

Figure 4: Reduction in liver pathology is AAV9 dose dependent.
(A) Cholesterol storage (filipin labeling) and CD68+ immunofluorescent staining in the liver (free floating sections) in 10-week-old mice. Arrows in high dose inset denote groups of cells without cholesterol storage. Scale bar for panel = 500 microns, insets scale bar = 50 microns. **(B)** CD68+ immunohistochemical staining of myeloid cells in livers of 10-week-old mice (free floating sections). Scale bar = 250 microns. **(C)** Quantification of percent area CD68 labelled in 10-week-old mice (One-way ANOVA with Tukey's multiple comparison' test) (saline n = 5, low n = 5, medium n = 6, high n = 6, *Npc1*$^{+/+}$ n = 9). For C: * P<0.05, ** P<0.01, *** P<0.001, **** P<0.0001, data presented as mean ± SD for C.

Figure 5: *Npc1*^{m1N} mice treated with medium dose AAV9 at 4 weeks old show increased survival, delayed weight loss, and slower disease progression than mice treated at 6 or 8 weeks old.
(A) Kaplan-Meier survival curve of mice treated with AAV9. **(B)** Table of median survival for each treatment group, significance (Mantel-Cox Log-Rank test) of data from (A) with Bonferroni's correction for 6 comparisons applied (P=0.0083). **(C)** Week at which mice reached peak weight. **(D)** Percent weight change between 6 and 9 weeks old. For C, D (saline n = 15, 4 weeks n = 24, 6 weeks n = 20, 8 weeks n = 20) for D (*Npc1*$^{+/+}$ n = 21) (one-way ANOVA with Tukey's multiple comparisons test). **(E)** Composite phenotype scores for each dosage group with measurements taken every 3 weeks, starting at 6 weeks (results presented in Fig S2B) (saline n = 14, 4 weeks n=13, 6 weeks n = 20, 8 weeks n = 20, *Npc1*$^{+/+}$ n = 21). For all: * P<0.05, ** P<0.01, *** P<0.001, **** P<0.0001. Data presented as mean ± SD for C, D, E.

Figure 6: Differential transduction efficacy of AAV9 gene therapy vector injected at varying time points in brain leads to differential amelioration of brain pathology.
(A) Linear regression of *hNPC1* copy number in end stage mice. (saline n = 14, 4-week n = 19, 6-week n = 20, 8-week n = 20, *Npc1*$^{+/+}$ n = 17). **(B)** ddPCR was used to measure gene copy number of *hNPC1* at 9 weeks old (One-way ANOVA with Tukey's multiple comparisons test) (saline n = 6, 4-week n = 3, 6-week n = 4, 8-week n = 4, *Npc1*$^{+/+}$ n = 4). **(C)** Purkinje neurons, labeled by Calbindin D (free floating sections). **(D)** Microgliosis, demonstrated by IBA1 staining (formalin-fixed, paraffin embedded sections). For (C, D): Scale bar = 1000 microns, insets scale bar = 250 microns. For B: * P<0.05, ** P<0.01, *** P<0.001, **** P<0.0001, data presented as mean ± SD.

Figure 7: *Npc1*^{I1061T} mice treated with AAV9 showed increased survival and growth.
(A) Kaplan Meier curve depicts survival of saline injected *Npc1*^{I1061T} mice (n = 11) and *Npc1*^{I1061T} mice treated with AAV9 at 4 weeks (n = 15). **(B)** Week mice reached peak weight (Wilcoxon test). **(C)** Percent weight change from 10 to 14 weeks (Kruskal-Wallis with Dunn's multiple comparisons). **(D)** Composite phenotype score for each group measured from 6 to 21 weeks at 3-week intervals. For B, C, D (saline n = 11, treated n = 15, *Npc1*$^{+/+}$ n = 15). For all: * P<0.05, ** P<0.01, *** P<0.001, **** P<0.0001. Data presented as mean ± SD.

SUPPLEMENTAL

Table S1: Number of mice used in each figure panel. For dose study and age of treatment, the same mice populations were used for *Npc1*^{m1N} injected with saline, *Npc1*^{m1N} medium dose treated at 4 weeks, and *Npc1*$^{+/+}$. Includes (n) for supplemental figures.

Table S2: Antibodies used for immunohistochemical and immunofluorescent staining along with manufacturer and dilution information.

S1: Mouse weights. *Npc1*^{m1N} mice treated with AAV9 vector and *Npc1*$^{+/+}$ mice weights over lifespan. For the dose study, **(A)** weights of males averaged with SD, **(B)** weights of females with SD. For age at injection: **(C)** males, **(D)** females. For *Npc1*^{I1061T} mice: **(E)** males, **(F)** females. (n) listed in figure.

S2: *Npc1*^{m1N} mice treated with AAV9 vector and *Npc1*$^{+/+}$ mice phenotype score comparison from 6-12 weeks. (A) Two-way ANOVA results of comparison of various dose treatment groups from 6-9 weeks, and 9-12 weeks. Results presented in table. **(B)** Two-way ANOVA results of comparison of various age treatment groups from 6-9 weeks, and 9-12 weeks. Results presented in table. For (A, B) Tukey's multiple comparisons test, level of significance is P=0.0083 based on Bonferroni's correction with 6 comparisons.

S3: Liver pathology and copy number variation of gene therapy treated mice at different ages.
(A) Linear regression between hNPC1 copy number and lifespan (saline n = 14, 4-week n = 18, 6-week n = 20, 8-week n = 20, *Npc1*$^{+/+}$ n = 17). **(B)** ddPCR was used to measure gene copy number of *hNPC1* at 9 weeks old. (One-way ANOVA with Tukey's multiple comparisons test) (saline n = 6, 4-week n = 4, 6-week n = 4, 8-week n = 4, *Npc1*$^{+/+}$ n = 4). **(C)** CD68+ labeling of Kupffer cells in the liver in 9-week-old mice. Scale bar = 250 microns. **(D)** Quantification of percent area CD68 labelled in 9-week-old mice (One-way ANOVA with Tukey's multiple comparisons test) (saline n = 6, 4-week n = 8, 6-week n = 4, 8-week n = 4, *Npc1*$^{+/+}$ n = 4). For all: * P<0.05, ** P<0.01, *** P<0.001, **** P<0.0001. Data presented as mean ± SD for B, D.

S4: **Transduction efficacy of AAV9 in *Npc1*^{I1061T} mice cerebrum and liver tissue.**
(A, C) ddPCR was used to measure gene copy number of *hNPC1* at end stage. Linear regression between *hNPC1* copy number and lifespan in cerebrum (A) or liver tissue (C). For A: (saline n = 11, treated n = 12, *Npc1*$^{+/+}$ n = 14), C: (saline n = 11, treated n = 13, *Npc1*$^{+/+}$ n = 14). **(B, D)** ddPCR was used to measure *hNPC1* copy number at 14 weeks. (B) *hNPC1* copy number per cell compared to *Npc1*$^{+/+}$ in the cerebrum. (D) *hNPC1* copy numbers in the liver compared to both saline treated mice and *Npc1*$^{+/+}$. For B, D: (One-Way ANOVA with Tukey's multiple comparisons test) (saline n = 4, treated n = 5, *Npc1*$^{+/+}$ n = 5). **(E)** Immunohistochemical staining of liver of *Npc1*$^{+/+}$, treated, and saline-injected 14-week-old mice. Scale bar = 250 microns. **(F):** Quantification of percent area CD68 labelled in 14-week-old mice (One-way ANOVA with Tukey's multiple comparisons test) (saline n = 5, treated n = 5, *Npc1*$^{+/+}$ n = 6). For all: * P<0.05, ** P<0.01, *** P<0.001, **** P<0.0001. Data presented as mean ± SD.

S5: Representative western blots: quantification of NPC1 in cerebrum and liver.
Representative western blots for quantification of NPC1 in cerebrum (A) and liver (B). Quantification of proteins are shown in Fig 2Aiii (cerebrum) and 2Biii (liver). Red outline denotes immunoreactive NPC1 protein. CNV of *hNPC1* provided for each sample below the blots. Source images for cerebrum (C) and liver (D).

S6. Representative western blots: quantification of GFAP and CD68 in cerebellum.

Representative western blots for quantification of GFAP (A) and CD68 (B) in cerebellum. Quantification of proteins are shown in Fig 3C and 3E, respectively. Red outlined denotes immunoreactive GFAP protein. CNV of *hNPC1* provided for each sample below the blots. Source images for cerebellum GFAP (C) and cerebellum CD68 (D).

S7. Representative western blots: quantification of calbindin D and NPC1 in cerebellum.
Representative western blot for quantification of calbindin D (A) and NPC1 (B) in cerebellum. Quantification of proteins are shown in Fig 3D and 3G, respectively. Red outline denotes immunoreactive NPC1 protein. CNV of *hNPC1* provided for each sample below the blots. Source image for cerebellum (C).

S8: Mass spectrometry imaging of *Npc1*$^{+/+}$ and *Npc1*^{m1N} mice treated with AAV9 gene therapy.
The lipids displayed include A) Ganglioside GM2 (d18:1/18:0), B) Hexosylceramide HexCer 46:4;O3, and C) Dihydroceramide Cer 32:2;O3.

REFERENCES

1. Vanier, M.T., *Niemann-Pick diseases.* Handb Clin Neurol, 2013. **113**: p. 1717-21.
2. Ory, D.S., *Niemann-Pick type C: a disorder of cellular cholesterol trafficking.* Biochim Biophys Acta, 2000. **1529**(1-3): p. 331-9.
3. Sleat, D.E., et al., *Genetic evidence for nonredundant functional cooperativity between NPC1 and NPC2 in lipid transport.* Proc Natl Acad Sci U S A, 2004. **101**(16): p. 5886-91.
4. Infante, R.E., et al., *Purified NPC1 protein. I. Binding of cholesterol and oxysterols to a 1278-amino acid membrane protein.* J Biol Chem, 2008. **283**(2): p. 1052-63.
5. Vanier, M.T., et al., *Genetic heterogeneity in Niemann-Pick C disease: a study using somatic cell hybridization and linkage analysis.* Am J Hum Genet, 1996. **58**(1): p. 118-25.
6. Cologna, S.M. and A. Rosenhouse-Dantsker, *Insights into the Molecular Mechanisms of Cholesterol Binding to the NPC1 and NPC2 Proteins.* Adv Exp Med Biol, 2019. **1135**: p. 139-160.
7. Vanier, M.T., *Niemann-Pick disease type C.* Orphanet J Rare Dis, 2010. **5**: p. 16.
8. Patterson, M.C., et al., *Recommendations for the diagnosis and management of Niemann-Pick disease type C: an update.* Mol Genet Metab, 2012. **106**(3): p. 330-44.
9. Fields, T., et al., *N-acetyl-L-leucine for Niemann-Pick type C: a multinational double-blind randomized placebo-controlled crossover study.* Trials, 2023. **24**(1): p. 361.
10. Mengel, E., et al., *Efficacy and safety of arimoclomol in Niemann-Pick disease type C: Results from a double-blind, randomised, placebo-controlled, multinational phase 2/3 trial of a novel treatment.* J Inherit Metab Dis, 2021. **44**(6): p. 1463-1480.
11. Patterson, M.C., et al., *Miglustat for treatment of Niemann-Pick C disease: a randomised controlled study.* Lancet Neurol, 2007. **6**(9): p. 765-72.
12. Ory, D.S., et al., *Intrathecal 2-hydroxypropyl-beta-cyclodextrin decreases neurological disease progression in Niemann-Pick disease, type C1: a non-randomised, open-label, phase 1-2 trial.* Lancet, 2017. **390**(10104): p. 1758-1768.
13. Patterson, M.C., et al., *Stable or improved neurological manifestations during miglustat therapy in patients from the international disease registry for Niemann-Pick disease type C: an observational cohort study.* Orphanet J Rare Dis, 2015. **10**: p. 65.
14. Solomon, B.I., et al., *Association of Miglustat With Swallowing Outcomes in Niemann-Pick Disease, Type C1.* JAMA Neurol, 2020. **77**(12): p. 1564-1568.
15. Mendell, J.R., et al., *Single-Dose Gene-Replacement Therapy for Spinal Muscular Atrophy.* N Engl J Med, 2017. **377**(18): p. 1713-1722.
16. Gao, J., R.M. Hussain, and C.Y. Weng, *Voretigene Neparvovec in Retinal Diseases: A Review of the Current Clinical Evidence.* Clin Ophthalmol, 2020. **14**: p. 3855-3869.
17. Al-Zaidy, S., et al., *Health outcomes in spinal muscular atrophy type 1 following AVXS-101 gene replacement therapy.* Pediatr Pulmonol, 2019. **54**(2): p. 179-185.
18. Hudry, E. and L.H. Vandenberghe, *Therapeutic AAV Gene Transfer to the Nervous System: A Clinical Reality.* Neuron, 2019. **102**(1): p. 263.
19. Lowes, L.P., et al., *Impact of Age and Motor Function in a Phase 1/2A Study of Infants With SMA Type 1 Receiving Single-Dose Gene Replacement Therapy.* Pediatr Neurol, 2019. **98**: p. 39-45.
20. Ali, H.G., et al., *Gene therapy for spinal muscular atrophy: the Qatari experience.* Gene Ther, 2021. **28**(10-11): p. 676-680.

21. Chandler, R.J., et al., *Systemic AAV9 gene therapy improves the lifespan of mice with Niemann-Pick disease, type C1.* Hum Mol Genet, 2017. **26**(1): p. 52-64.
22. Cain, J.T., et al., *Gene Therapy Corrects Brain and Behavioral Pathologies in CLN6-Batten Disease.* Mol Ther, 2019. **27**(10): p. 1836-1847.
23. Bosch, M.E., et al., *Self-Complementary AAV9 Gene Delivery Partially Corrects Pathology Associated with Juvenile Neuronal Ceroid Lipofuscinosis (CLN3).* J Neurosci, 2016. **36**(37): p. 9669-82.
24. Sondhi, D., et al., *Slowing late infantile Batten disease by direct brain parenchymal administration of a rh.10 adeno-associated virus expressing CLN2.* Sci Transl Med, 2020. **12**(572).
25. Manfredsson, F.P., A.C. Rising, and R.J. Mandel, *AAV9: a potential blood-brain barrier buster.* Mol Ther, 2009. **17**(3): p. 403-5.
26. Foust, K.D., et al., *Intravascular AAV9 preferentially targets neonatal neurons and adult astrocytes.* Nat Biotechnol, 2009. **27**(1): p. 59-65.
27. Lykken, E.A., et al., *Recent progress and considerations for AAV gene therapies targeting the central nervous system.* J Neurodev Disord, 2018. **10**(1): p. 16.
28. Verdera, H.C., K. Kuranda, and F. Mingozzi, *AAV Vector Immunogenicity in Humans: A Long Journey to Successful Gene Transfer.* Mol Ther, 2020. **28**(3): p. 723-746.
29. Bradbury, A.M., et al., *Krabbe disease successfully treated via monotherapy of intrathecal gene therapy.* J Clin Invest, 2020. **130**(9): p. 4906-4920.
30. Bagel, J.H., et al., *Electrodiagnostic testing and histopathologic changes confirm peripheral nervous system myelin abnormalities in the feline model of niemann-pick disease type C.* J Neuropathol Exp Neurol, 2013. **72**(3): p. 256-62.
31. Xie, C., et al., *AAV9-NPC1 significantly ameliorates Purkinje cell death and behavioral abnormalities in mouse NPC disease.* J Lipid Res, 2017. **58**(3): p. 512-518.
32. Hughes, M.P., et al., *AAV9 intracerebroventricular gene therapy improves lifespan, locomotor function and pathology in a mouse model of Niemann-Pick type C1 disease.* Hum Mol Genet, 2018. **27**(17): p. 3079-3098.
33. Davidson, C.D., et al., *Improved systemic AAV gene therapy with a neurotrophic capsid in Niemann-Pick disease type C1 mice.* Life Sci Alliance, 2021. **4**(10).
34. Kurokawa, Y., et al., *Gene Therapy in a Mouse Model of Niemann-Pick Disease Type C1.* Hum Gene Ther, 2021. **32**(11-12): p. 589-598.
35. Hughes, M.P., et al., *A Novel Small NPC1 Promoter Enhances AAV-Mediated Gene Therapy in Mouse Models of Niemann-Pick Type C1 Disease.* Cells, 2023. **12**(12).
36. Tai, C.H., et al., *Long-term efficacy and safety of eladocagene exuparvovec in patients with AADC deficiency.* Mol Ther, 2022. **30**(2): p. 509-518.
37. Wasserstein, M.P., et al., *The future of newborn screening for lysosomal disorders.* Neurosci Lett, 2021. **760**: p. 136080.
38. Patterson, M.C., et al., *Disease and patient characteristics in NP-C patients: findings from an international disease registry.* Orphanet J Rare Dis, 2013. **8**: p. 12.
39. Surmeli-Onay, O., et al., *Prenatal-onset Niemann-Pick type C disease with nonimmune hydrops fetalis.* Pediatr Neonatol, 2013. **54**(5): p. 344-7.
40. Kelly, D.A., et al., *Niemann-Pick disease type C: diagnosis and outcome in children, with particular reference to liver disease.* J Pediatr, 1993. **123**(2): p. 242-7.

41. Kumagai, T., et al., *A case of Niemann-Pick disease type C with neonatal liver failure initially diagnosed as neonatal hemochromatosis.* Brain Dev, 2019. **41**(5): p. 460-464.
42. Shammas, H., et al., *Different Niemann-Pick C1 Genotypes Generate Protein Phenotypes that Vary in their Intracellular Processing, Trafficking and Localization.* Sci Rep, 2019. **9**(1): p. 5292.
43. Landrum, M.J., et al., *ClinVar: public archive of relationships among sequence variation and human phenotype.* Nucleic Acids Res, 2014. **42**(Database issue): p. D980-5.
44. McKay Bounford, K. and P. Gissen, *Genetic and laboratory diagnostic approach in Niemann Pick disease type C.* J Neurol, 2014. **261 Suppl 2**(Suppl 2): p. S569-75.
45. Millat, G., et al., *Niemann-Pick C1 disease: the I1061T substitution is a frequent mutant allele in patients of Western European descent and correlates with a classic juvenile phenotype.* Am J Hum Genet, 1999. **65**(5): p. 1321-9.
46. Guatibonza Moreno, P., et al., *At a glance: the largest Niemann-Pick type C1 cohort with 602 patients diagnosed over 15 years.* Eur J Hum Genet, 2023. **31**(10): p. 1108-1116.
47. Praggastis, M., et al., *A murine Niemann-Pick C1 I1061T knock-in model recapitulates the pathological features of the most prevalent human disease allele.* J Neurosci, 2015. **35**(21): p. 8091-106.
48. Gelsthorpe, M.E., et al., *Niemann-Pick type C1 I1061T mutant encodes a functional protein that is selected for endoplasmic reticulum-associated degradation due to protein misfolding.* J Biol Chem, 2008. **283**(13): p. 8229-36.
49. Yerger, J., et al., *Phenotype assessment for neurodegenerative murine models with ataxia and application to Niemann-Pick disease, type C1.* Biol Open, 2022. **11**(4).
50. Martin, K.B., et al., *Identification of Novel Pathways Associated with Patterned Cerebellar Purkinje Neuron Degeneration in Niemann-Pick Disease, Type C1.* Int J Mol Sci, 2019. **21**(1).
51. Boenzi, S., et al., *Comprehensive-targeted lipidomic analysis in Niemann-Pick C disease.* Mol Genet Metab, 2021. **134**(4): p. 337-343.
52. Pergande, M.R., et al., *Lipidomic Analysis Reveals Altered Fatty Acid Metabolism in the Liver of the Symptomatic Niemann-Pick, Type C1 Mouse Model.* Proteomics, 2019. **19**(18): p. e1800285.
53. Zervas, M., K. Dobrenis, and S.U. Walkley, *Neurons in Niemann-Pick disease type C accumulate gangliosides as well as unesterified cholesterol and undergo dendritic and axonal alterations.* J Neuropathol Exp Neurol, 2001. **60**(1): p. 49-64.
54. Rodriguez-Gil, J.L., et al., *Genetic background modifies phenotypic severity and longevity in a mouse model of Niemann-Pick disease type C1.* Dis Model Mech, 2020. **13**(3).

Figure 1

A

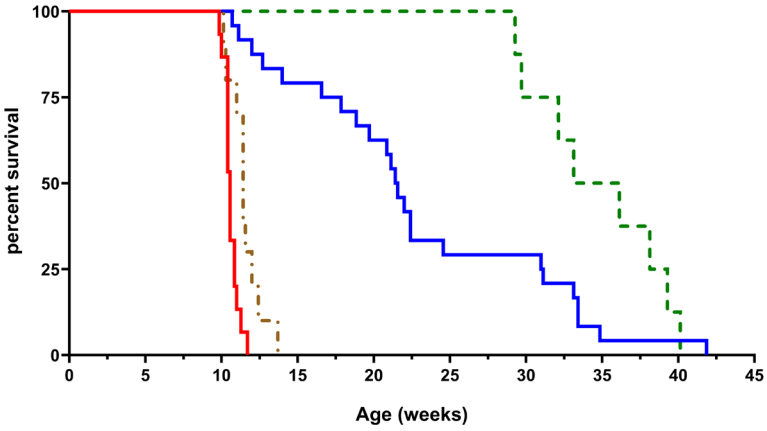

B

Treatment	Sample Size (n)	Median Survival (weeks)	Significance (Log-rank test)
Npc1^{m1N} Saline	15	10.6	
Npc1^{m1N} Low 7.87×10^{12} vg/kg	10	11.4	vs. Saline, ***P=0.0049***
Npc1^{m1N} Medium 1.28×10^{14} vg/kg	24	21.5	vs. Saline, ***P<0.0001*** vs. Low, ***P<0.0001***
Npc1^{m1N} High 3.06×10^{14} vg/kg	8	34.6	vs. Saline, ***P<0.0001*** vs. Low, ***P<0.0001*** vs. Medium, P=0.0266

C

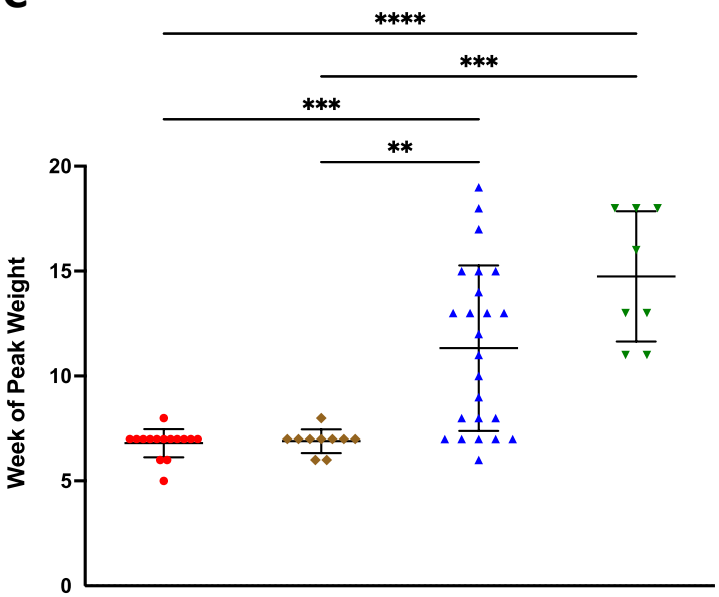

D

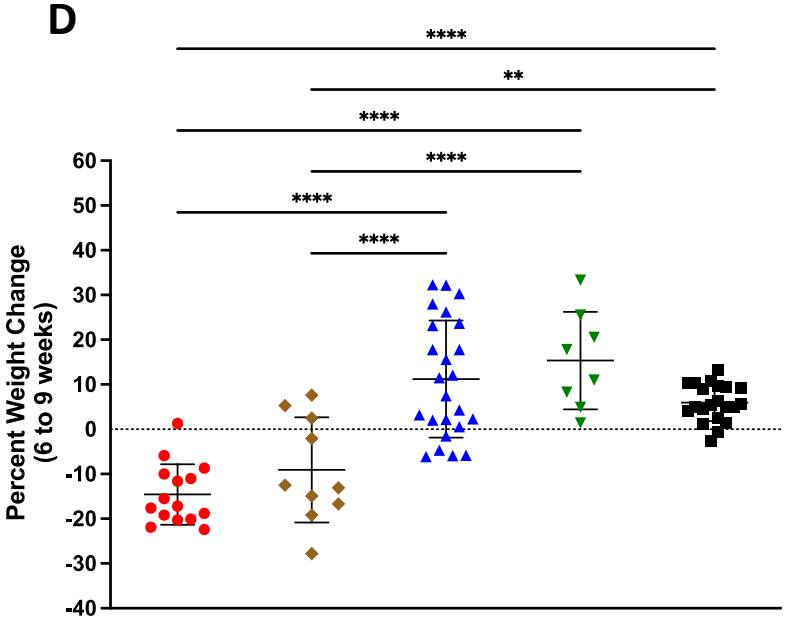

E

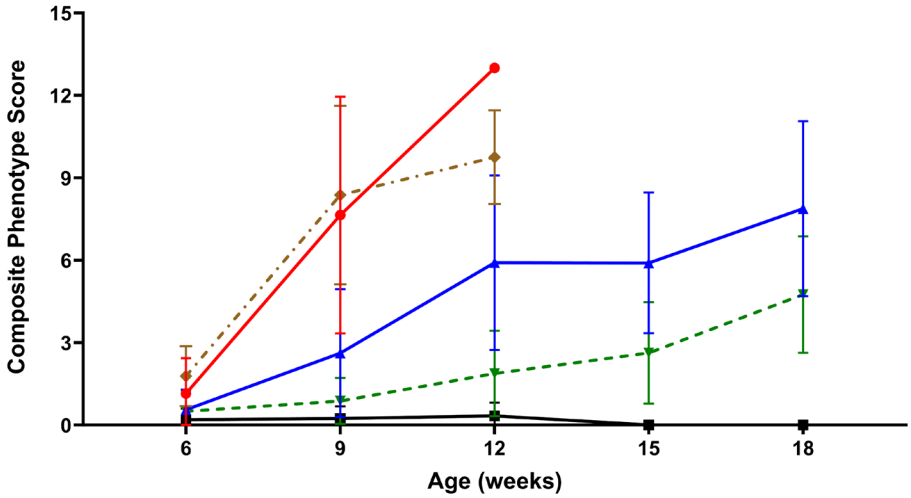

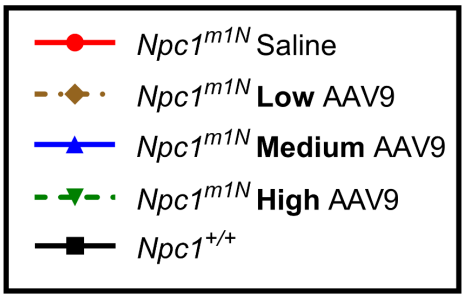

Figure 2

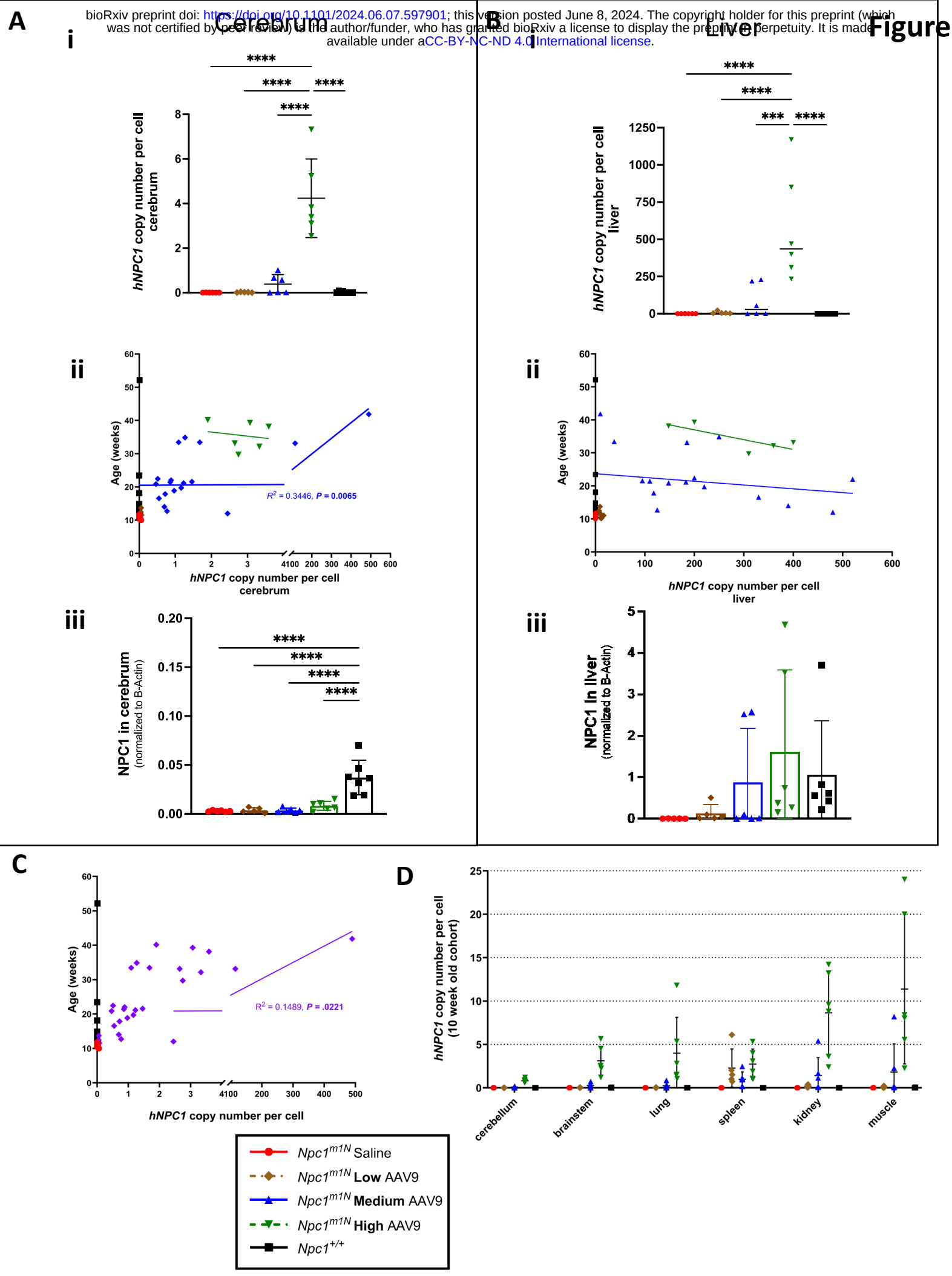

Figure 3

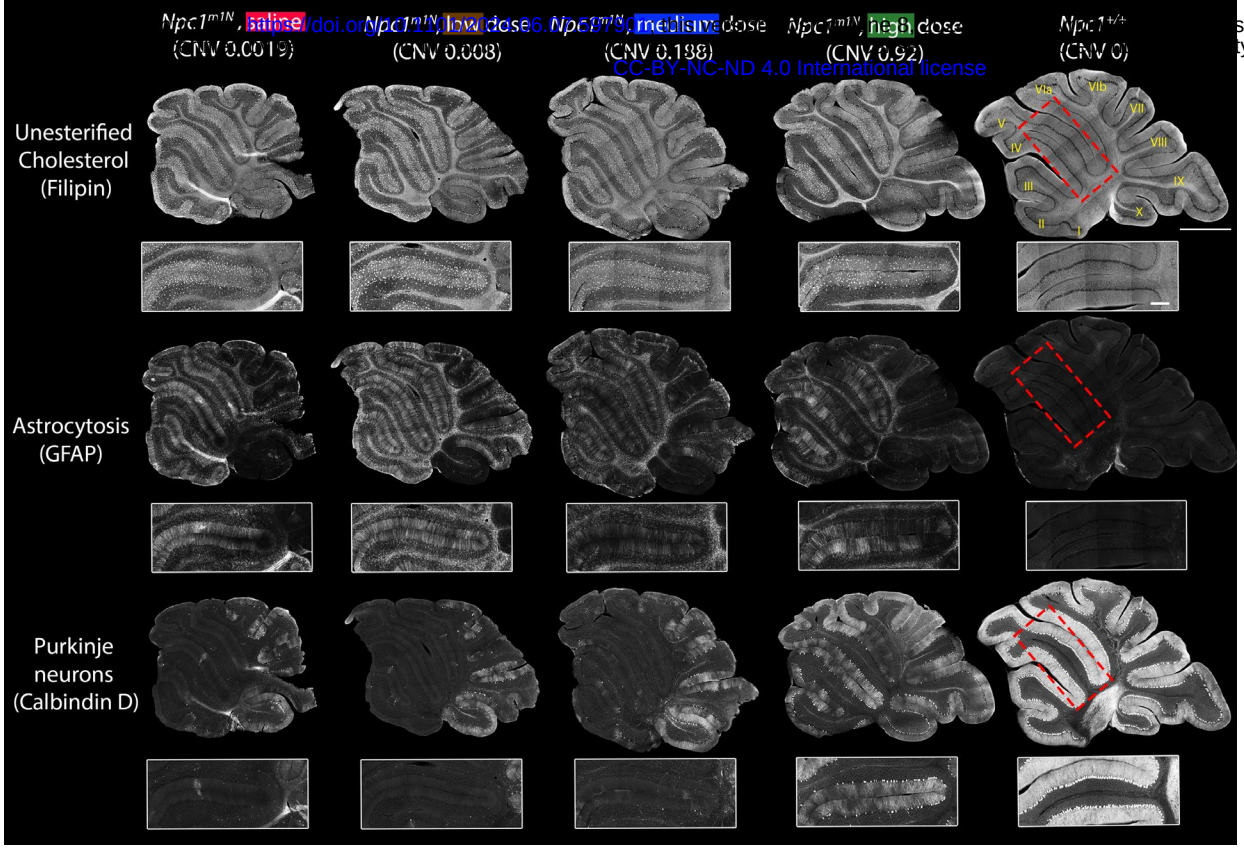

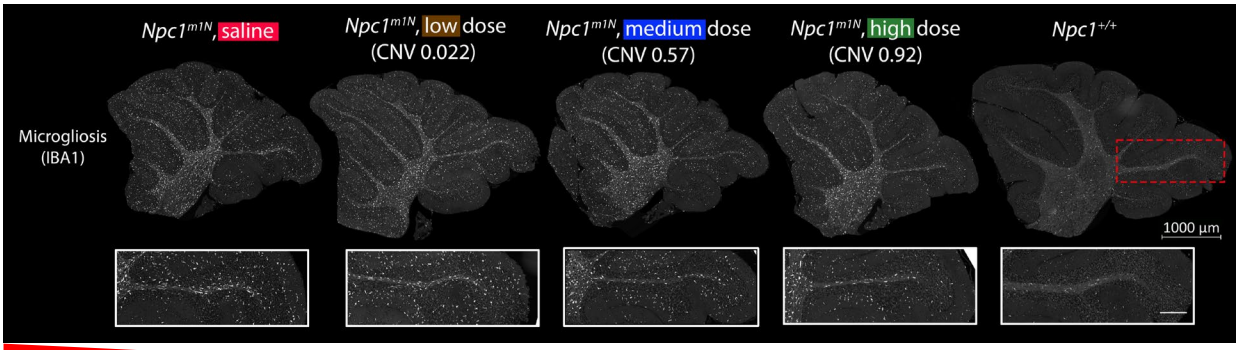

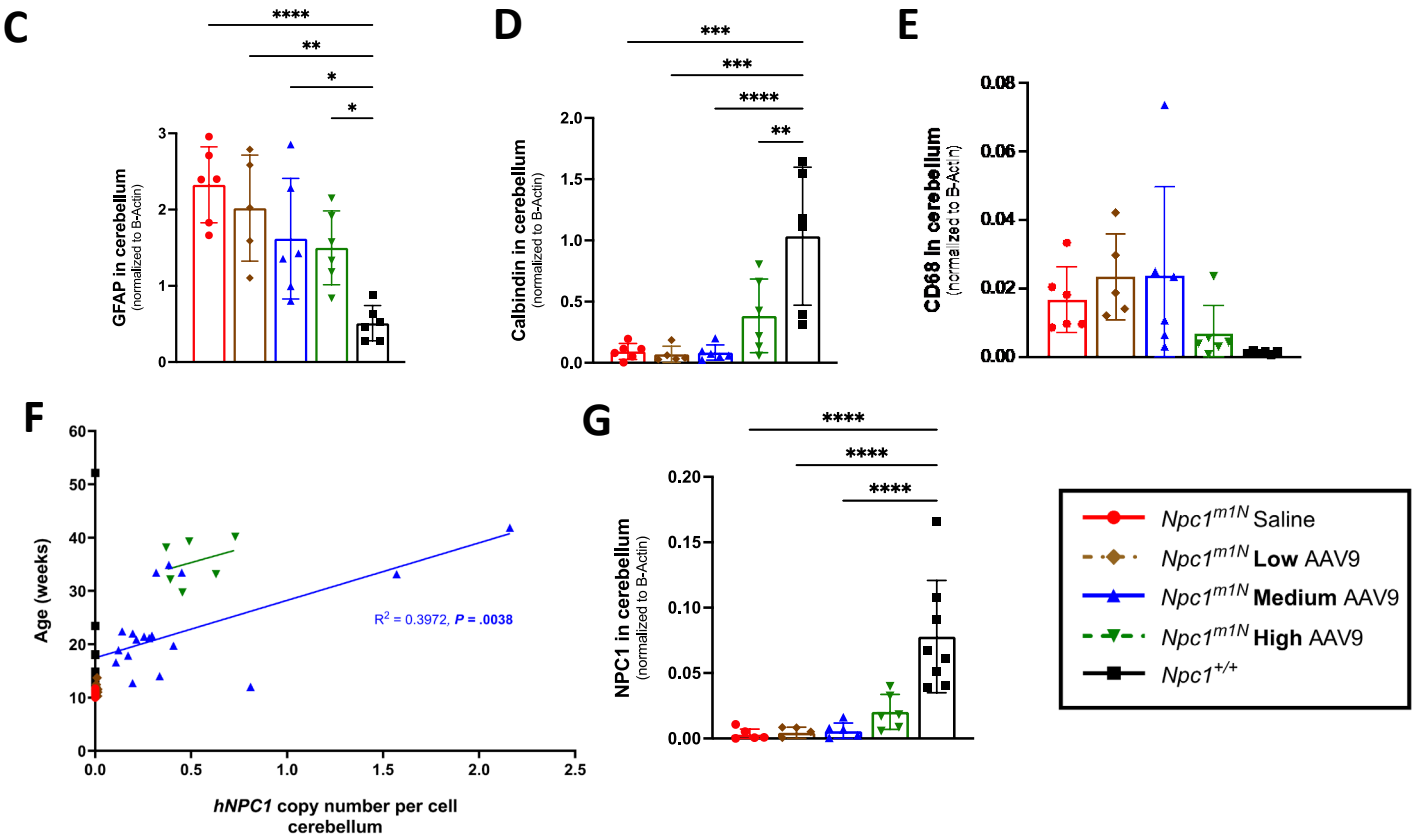

Figure 4

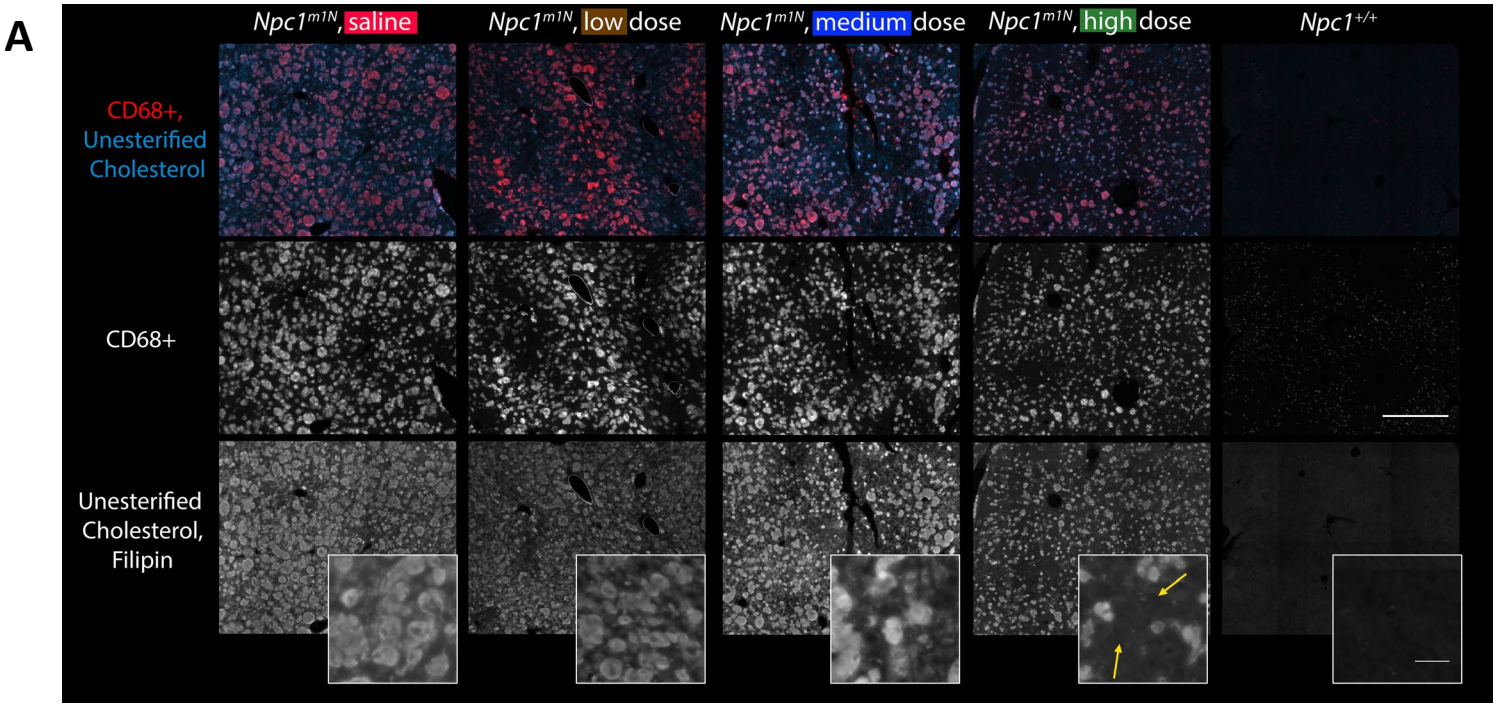

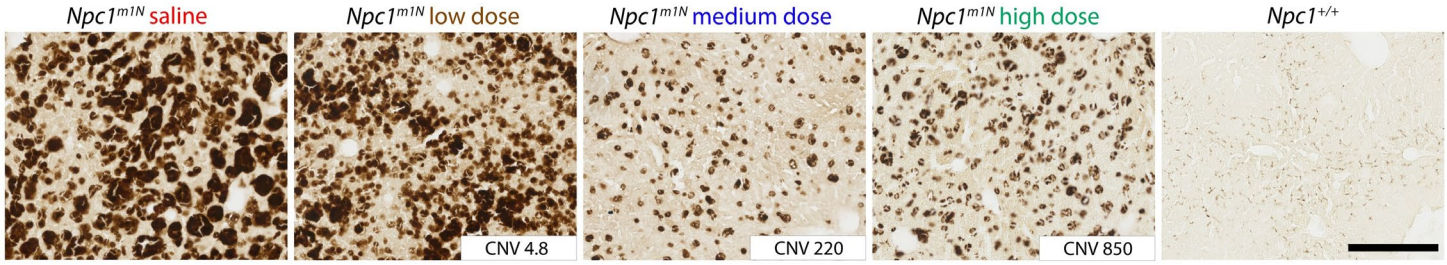

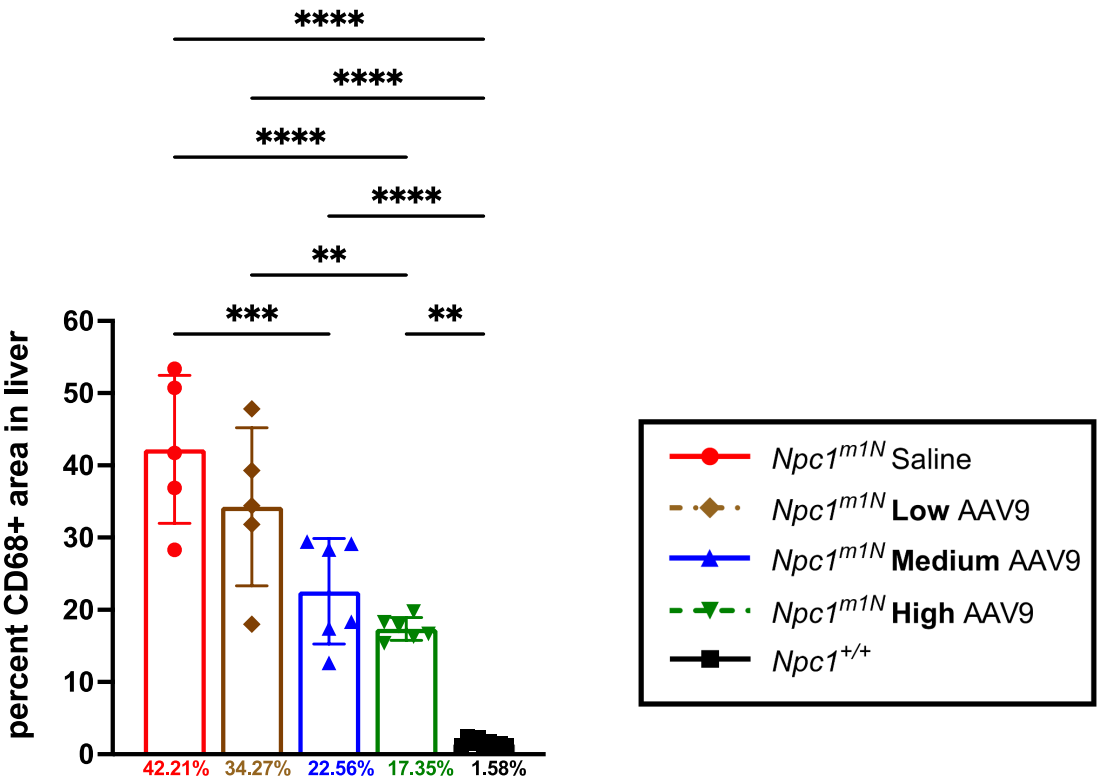

Figure 5

A

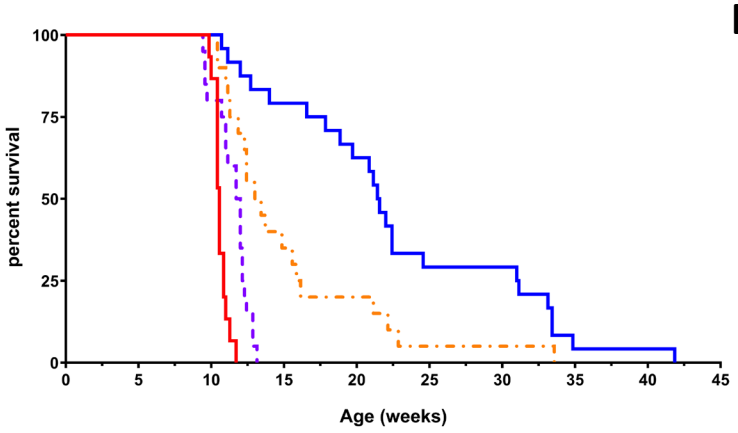

B

Treatment	Sample Size (n)	Median Survival (weeks)	Significance (Log-rank test)
Npc1^{m1N} Saline	15	10.6	
Npc1^{m1N} Med AAV9 at **4 weeks old**	24	21.5	vs. Saline, ***P<0.0001***
Npc1^{m1N} Med AAV9 at **6 weeks old**	20	13.2	vs. Saline, ***P<0.0001*** vs. 4 weeks old, ***P=0.0030***
Npc1^{m1N} Med AAV9 at **8 weeks old**	20	11.9	vs. Saline, ***P=0.0006*** vs. 4 weeks old, ***P<0.0001*** vs. 6 weeks old, ***P=0.0003***

C

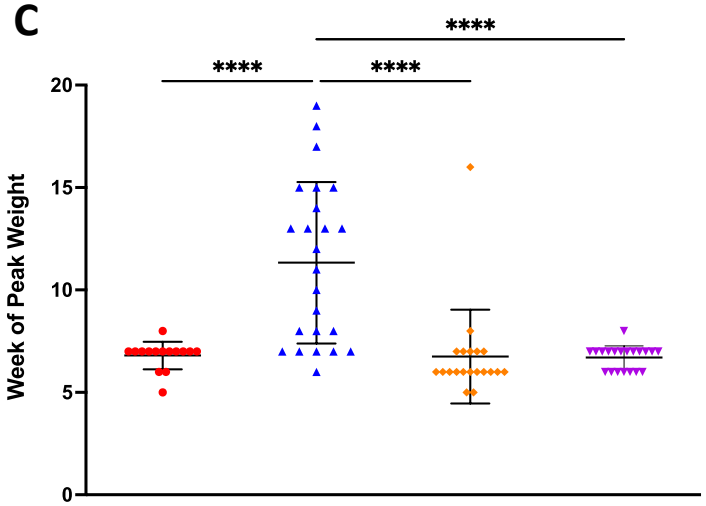

D

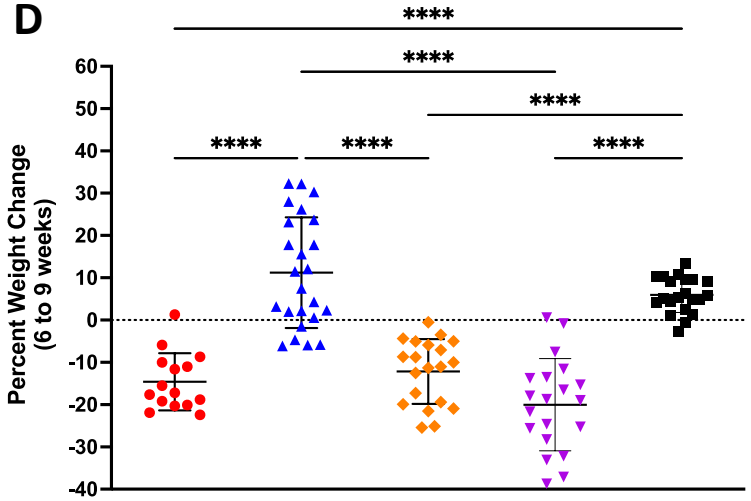

E

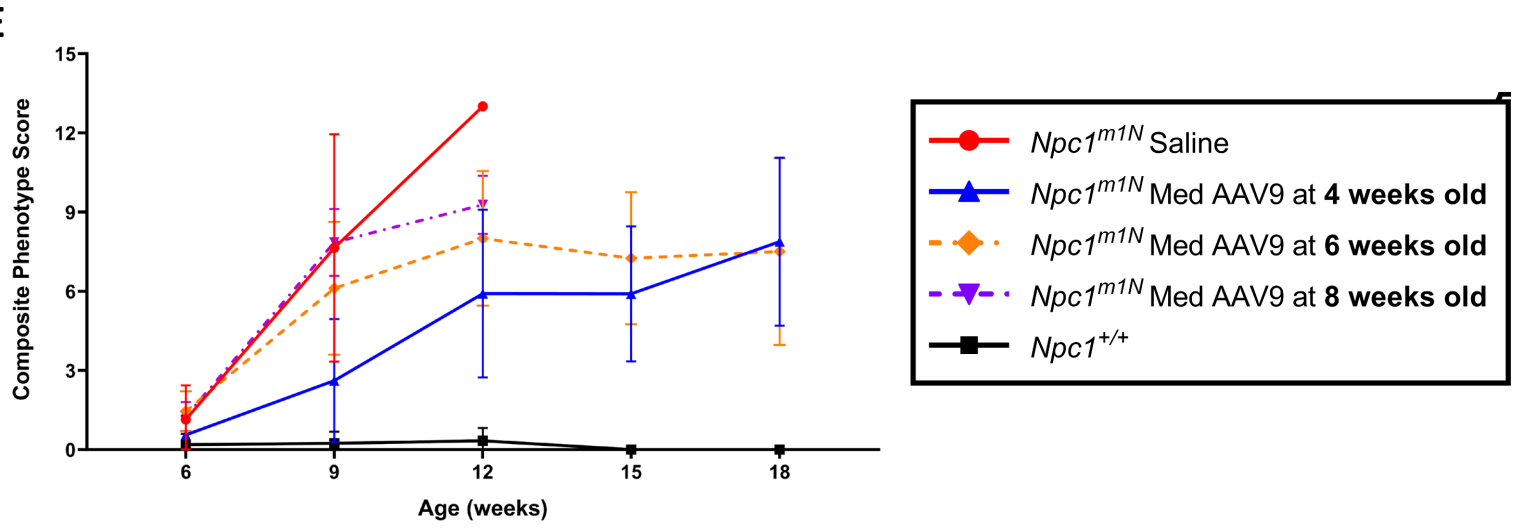

Figure 6

A

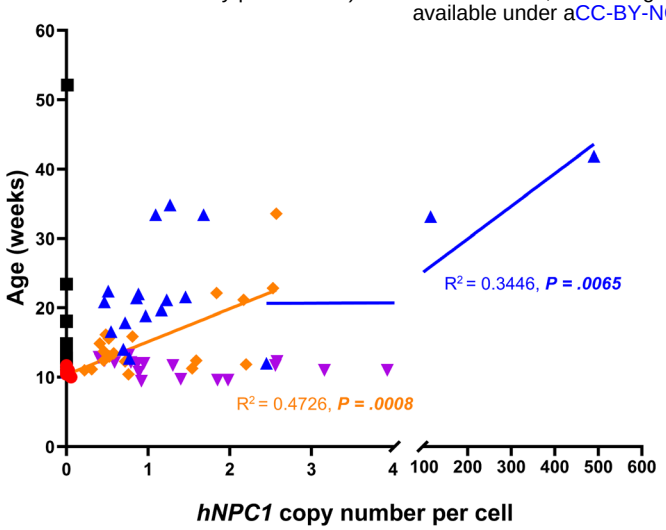

B

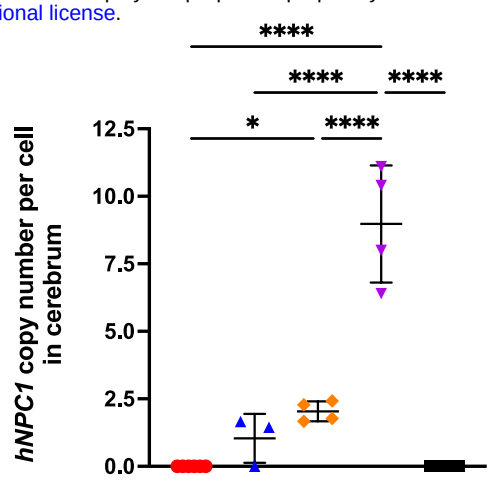

C

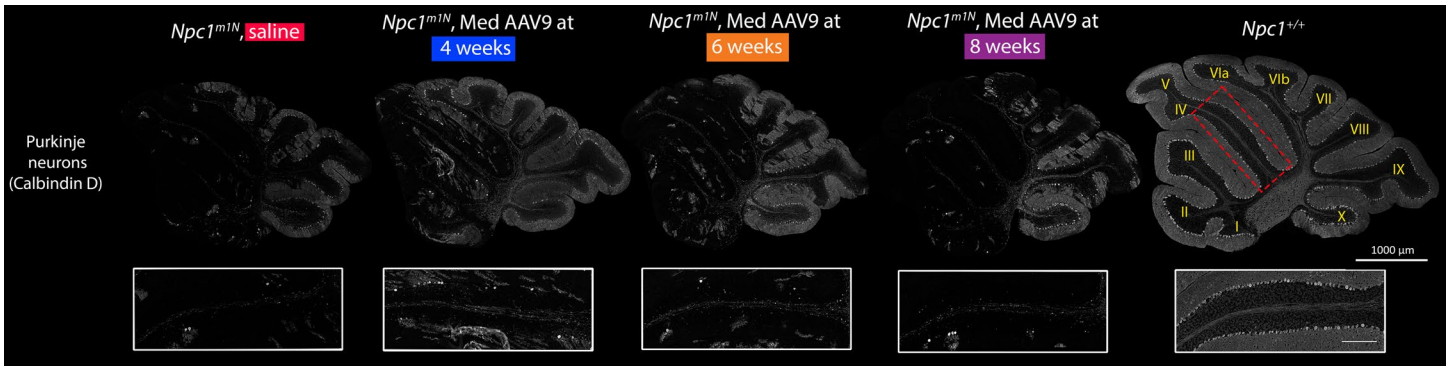

D

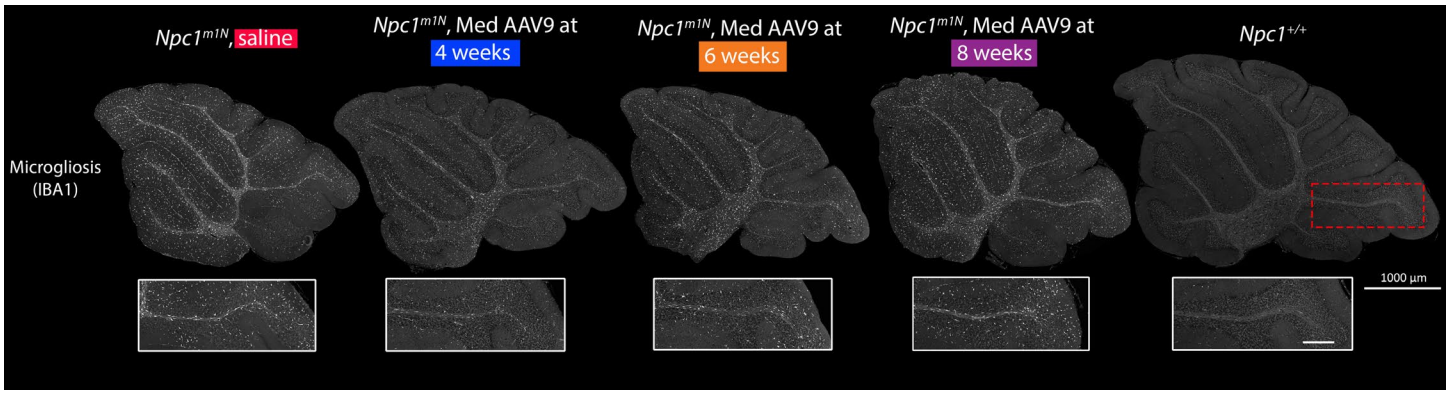

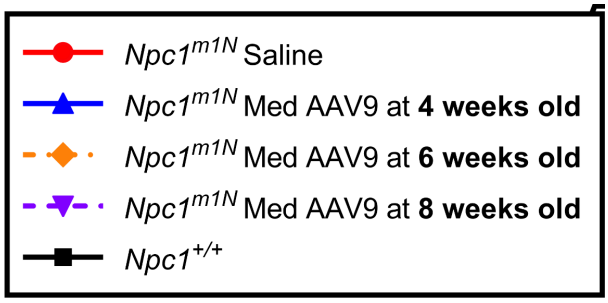

Figure 7

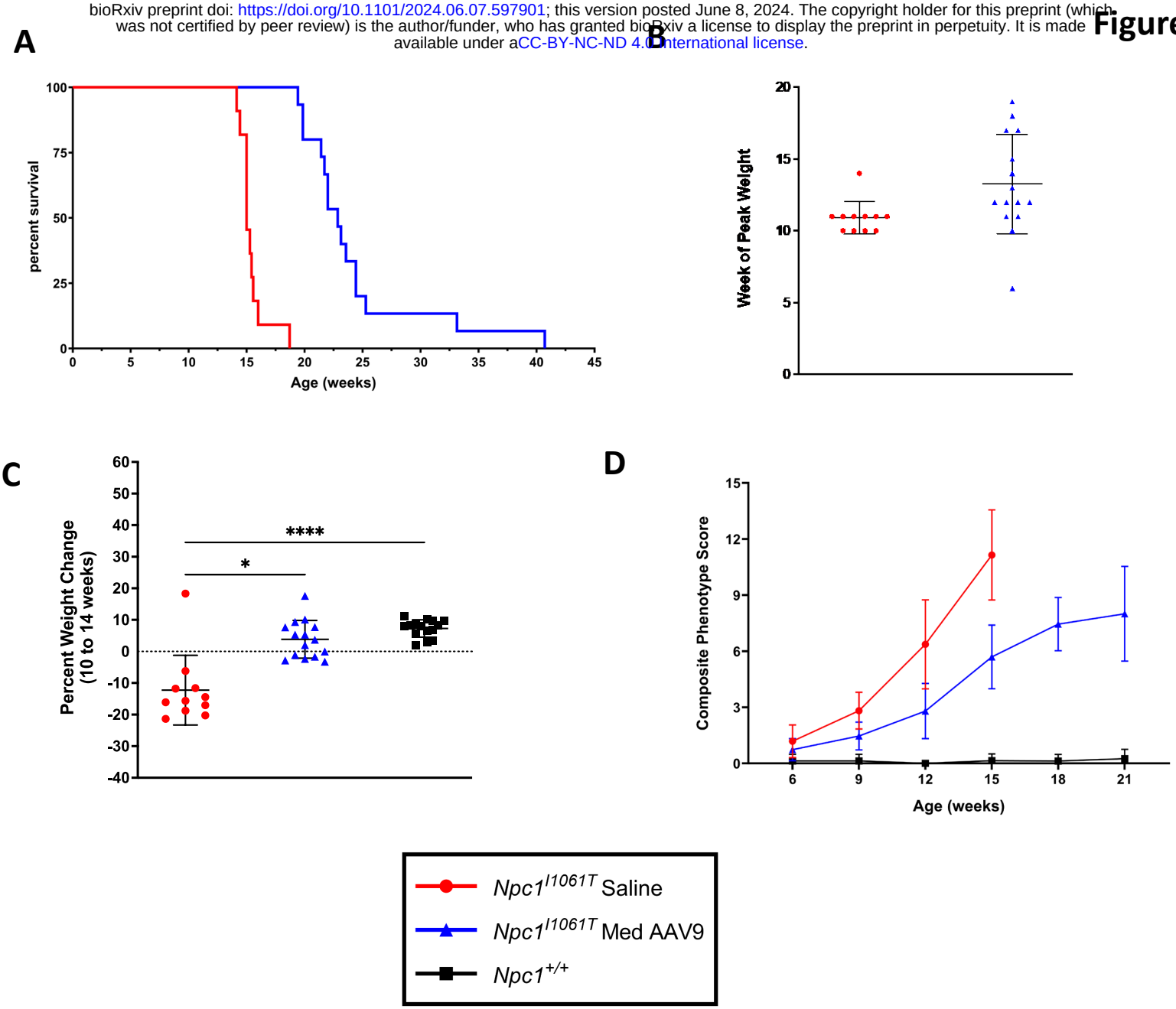

Table S1

Figure #		$Npc1^{m1N}$, saline	$Npc1^{m1N}$, low	$Npc1^{m1N}$, medium	$Npc1^{m1N}$, high	$Npc1^{+/+}$
1	C	15	10	24	8	
	D	15	10	24	8	21
2	A	14	9	20	6	17
	B	6	5	6	5	9
	C	5	5	6	6	7
	D	14	9	18	5	17
	E	6	5	6	6	9
	F	5	5	6	6	6
	G	8		34		16
	H	6	5	6	6	9
3	C	6	5	6	6	8
	D	6	5	6	6	8
	E	6	5	6	6	8
	F	14	9	20	6	17
	G	5	5	6	6	7
4	C	5	5	6	6	9
S1	A	8	6	10	4	11
	B	7	4	14	4	10
		$Npc1^{m1N}$, saline	$Npc1^{m1N}$, 4 weeks	$Npc1^{m1N}$, 6 weeks	$Npc1^{m1N}$, 8 weeks	$Npc1^{+/+}$
5	C	15	24	20	20	
	D	15	24	20	20	21
6	A	14	20	20	20	17
	B	6	3	3	4	4
S1	C	8	10	11	12	11
	D	7	14	9	8	10
S3	A	14	18	20	20	17
	B	6	4	4	4	4
	D	6	7	4	4	4
		$Npc1^{I1061T/I1061T}$, saline	$Npc1^{I1061T/I1061T}$, medium	$Npc1^{+/+}$		
7	C	11	15			
	D	11	15	25		
	E	11	15	15		
	F	5	5	6		
S4	A	11	12	14		
	B	7	5	6		
	C	11	13	14		
	D	7	5	6		

Table S2

Antibody	Company	Catalog Number	Dilution	Method
α-β-actin (mouse IgG)	ThermoFisher Invitrogen	15G5A11/E2	1:10000	Westerns
α-Calbindin (mouse IgG)	Sigma	C9848	1:750 1:1000	IF Westerns
α-Calbindin (rabbit IgG)	Abcam	ab229915	1:750 (fixed, free-floating sections and FFPE sections)	IF
α-CD68 (rat IgG2a)	BioRad	MCA1957	1:500	IF
α-CD68 (rabbit IgG)	Abcam	ab125212	1:1000	IHC, IF, Westerns
α-GFAP (mouse IgG)	Sigma	G3893	1:1000 (fixed, free-floating sections and FFPE sections) 1:2000	IF Westerns
α-IBA1 (rabbit IgG)	Wako Chemicals	019-19741	1:500 (fixed, free-floating sections) or 1:750 (FFPE)	IF
α-NPC1 (monoclonal rabbit IgG)	Abcam	ab134113	1:2000	Westerns
α-β-III-Tubulin	R&D Systems	MAB1195	1:3000	Westerns
Donkey anti-mouse IgG IRDye 680RD	LI-CORbio	926-68072	1:20000	Westerns
Donkey anti-mouse IgG IRDye 800CW	LI-CORbio	926-32213	1:20000	Westerns
Goat anti-rabbit IgG Biotinylated	Vector Laboratories	BA-1000	1:300	IHC
Goat anti-mouse IgG AlexaFluor 488 or 594	ThermoFisher Invitrogen	A11029 (488) or A11005 (594)	1:350	IF
Goat anti-rabbit IgG AlexaFluor 488 or 594	ThermoFisher Invitrogen	A11034 (488) or A11037 (594)	1:350	IF
Goat anti-rat IgG Alexa Fluor 488 or 594	ThermoFisher Invitrogen	A11006 (488) or A11007 (594)	1:350	IF

Figure S1

A

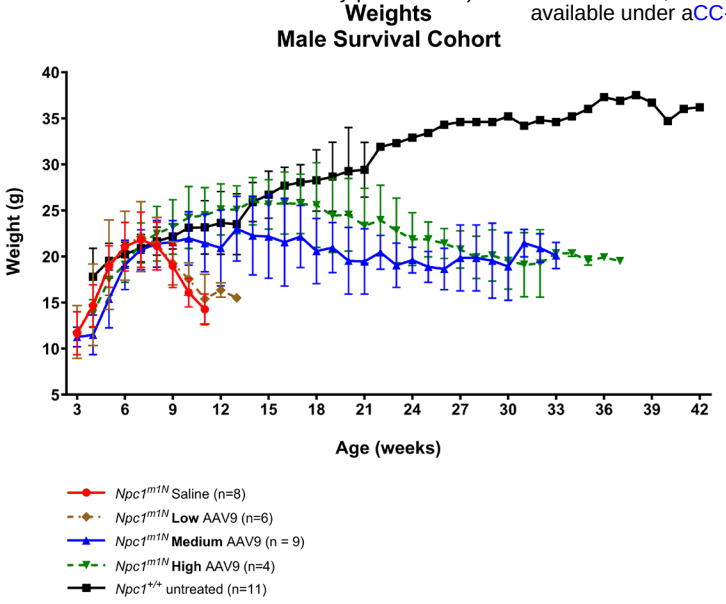

B

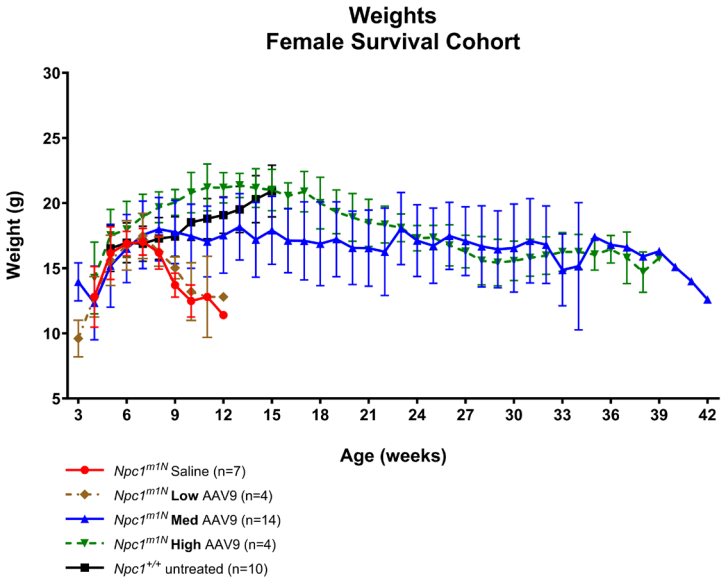

C

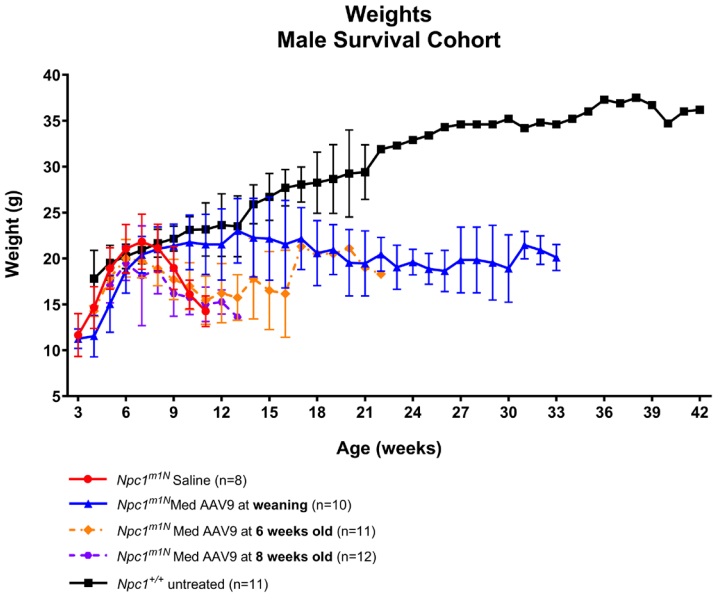

D

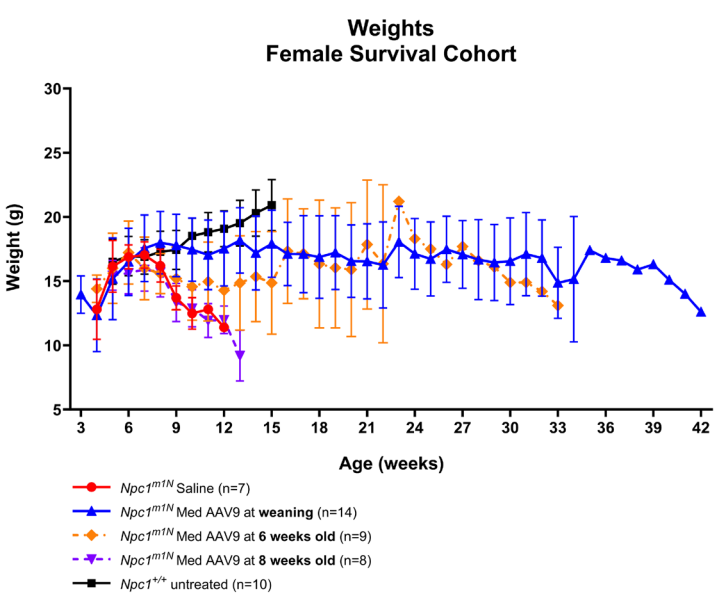

E

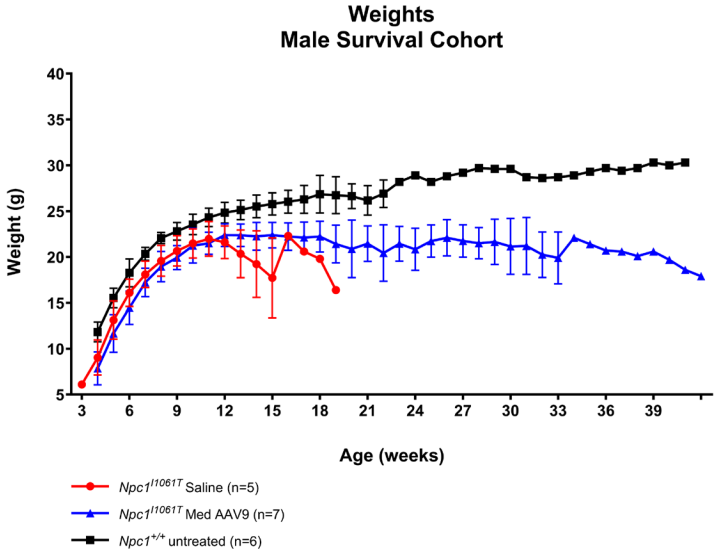

F

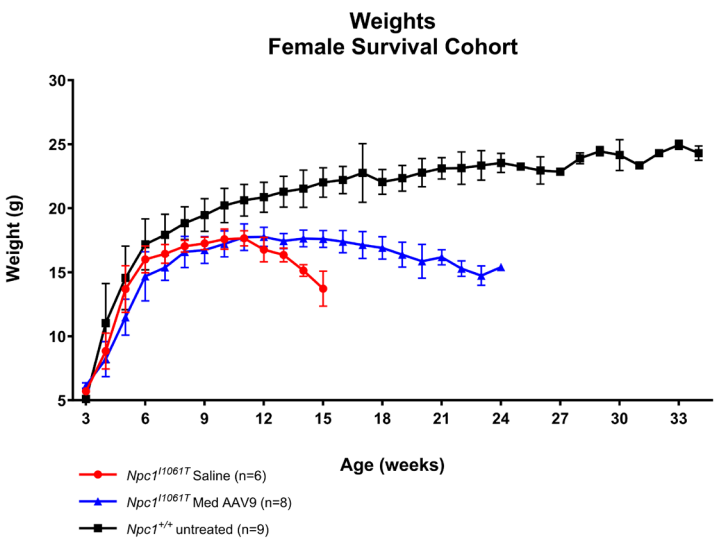

Figure S2

A

Treatment	Sample Size (n)	Significance (Tukey's Multiple Comparisons Test, 6-9 weeks)	Significance (Tukey's Multiple Comparisons Test, 9-12 weeks)
Npc1^{m1N} Saline	14		
Npc1^{m1N} Low	10	vs. Saline, P=0.9466	vs. Saline, P=0.9976
Npc1^{m1N} Medium	13	vs. Saline, P=0.0196 vs. Low, ***P=0.0069***	vs. Saline, ***P<0.0001*** vs. Low, ***P<0.0001***
Npc1^{m1N} High	8	vs. Saline, ***P<0.0001*** vs. Low, ***P<0.0001*** vs. Medium, P = 0.0129	vs. Saline, ***P<0.0001*** vs. Low, ***P<0.0001*** vs. Medium, **P = 0.0009**
Npc1$^{+/+}$	21	vs. Saline, ***P<0.0001*** vs. Low, ***P<0.0001*** vs. Medium, ***P = 0.0003*** vs. High, P = 0.9104	vs. Saline, ***P<0.0001*** vs. Low, ***P<0.0001*** vs. Medium, ***P<0.0001*** vs. High, P = 0.5073

B

Treatment	Sample Size (n)	Significance (Tukey's Multiple Comparisons Test, 6-9 weeks)	Significance (Tukey's Multiple Comparisons Test, 9-12 weeks)
Npc1^{m1N} Saline	14		
Npc1^{m1N} Med AAV9 at **4 weeks old**	13	vs. Saline, ***P<0.0001***	vs. Saline, ***P<0.0001***
Npc1^{m1N} Med AAV9 at **6 weeks old**	20	vs. Saline, P=0.7788 vs. 4 weeks old, ***P=0.0010***	vs. Saline, P=0.1909 vs. 4 weeks old, ***P=0.0002***
Npc1^{m1N} Med AAV9 at **8 weeks old**	20	vs. Saline, P=0.9984 vs. 4 weeks old, ***P<0.0001*** vs. 6 weeks old, P=0.5116	vs. Saline, P>0.9999 vs. 4 weeks old, ***P<0.0001*** vs. 6 weeks old, P=0.0.0747
Npc1$^{+/+}$	21	vs. Saline, ***P<0.0001*** vs. Weaning, P=0.2389 vs. 6 weeks old, ***P<0.0001*** vs. 8 weeks old, ***P<0.0001***	vs. Saline, ***P<0.0001*** vs. Weaning, ***P<0.0001*** vs. 6 weeks old, ***P<0.0001*** vs. 8 weeks old, ***P<0.0001***

Figure S3

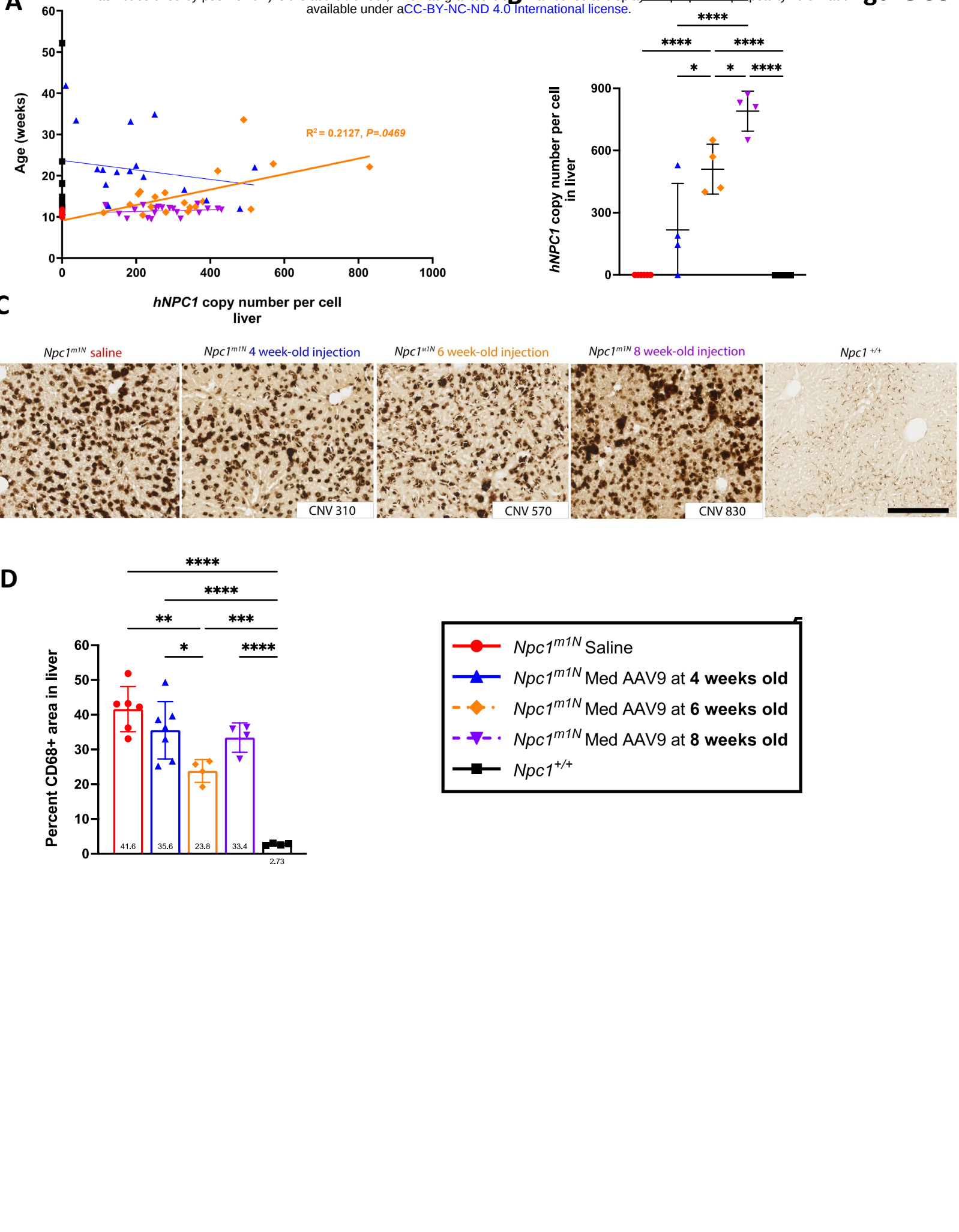

Figure S4

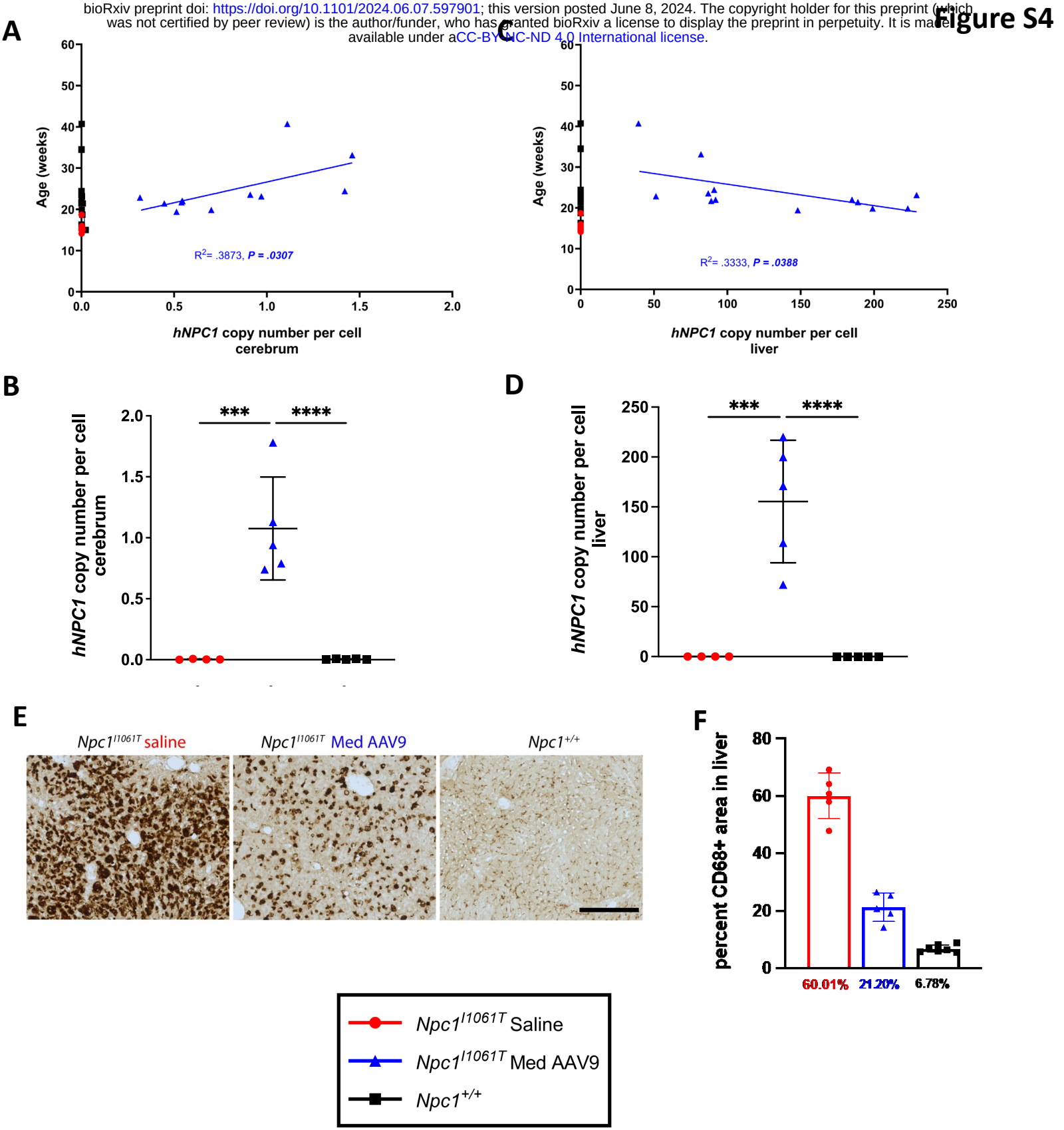

A

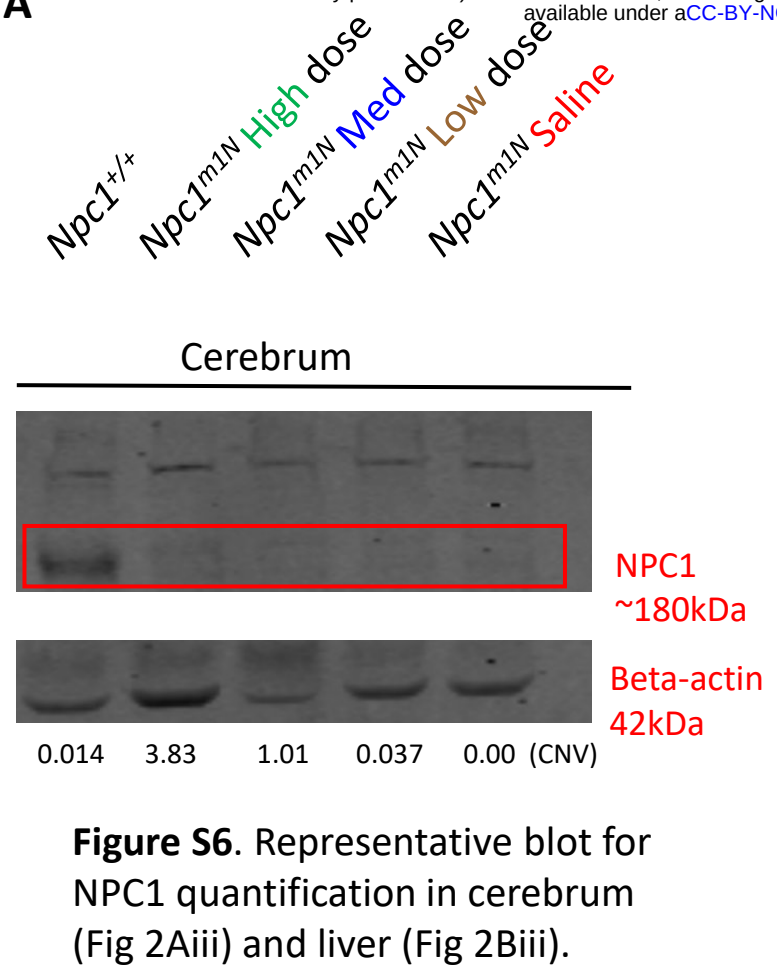

B

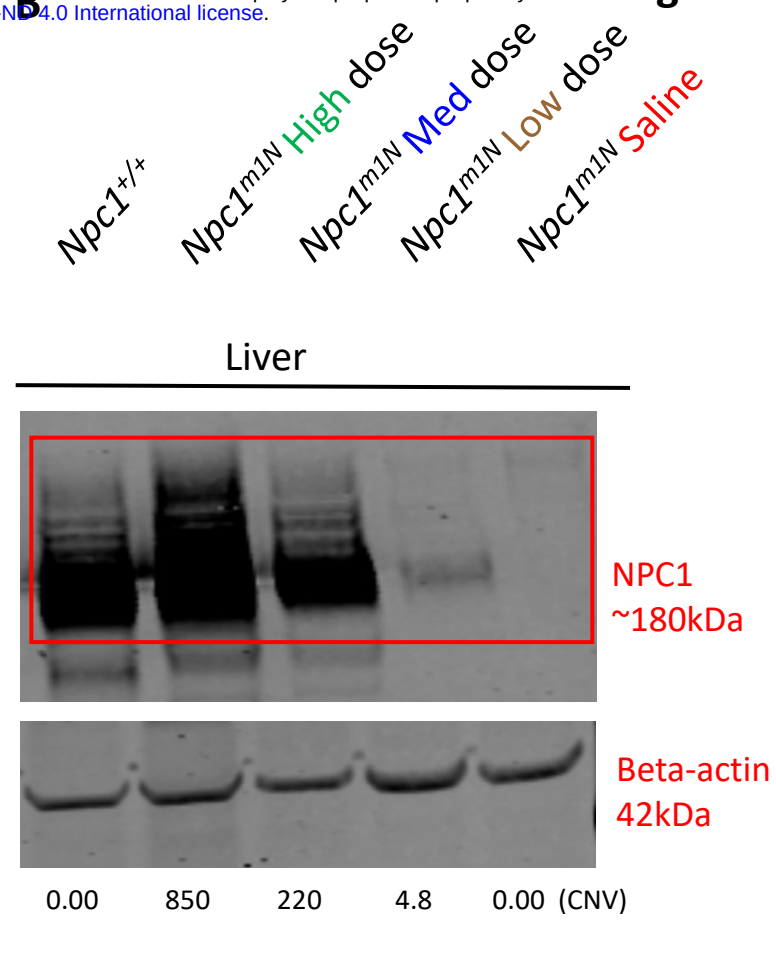

Figure S6. Representative blot for NPC1 quantification in cerebrum (Fig 2Aiii) and liver (Fig 2Biii). *hNPC1* copy number variation listed under blots for each sample.

C Original source data, cerebrum (NPC1, beta-actin; left half of blot enlarged).

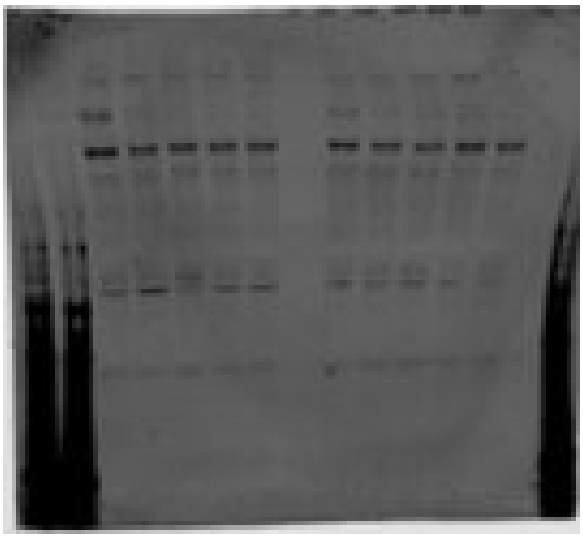

D Original source data, liver (NPC1, beta-actin; right half of blot enlarged).

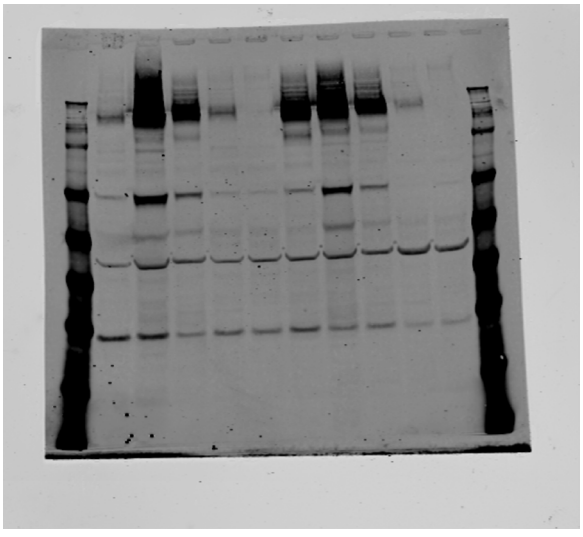

A

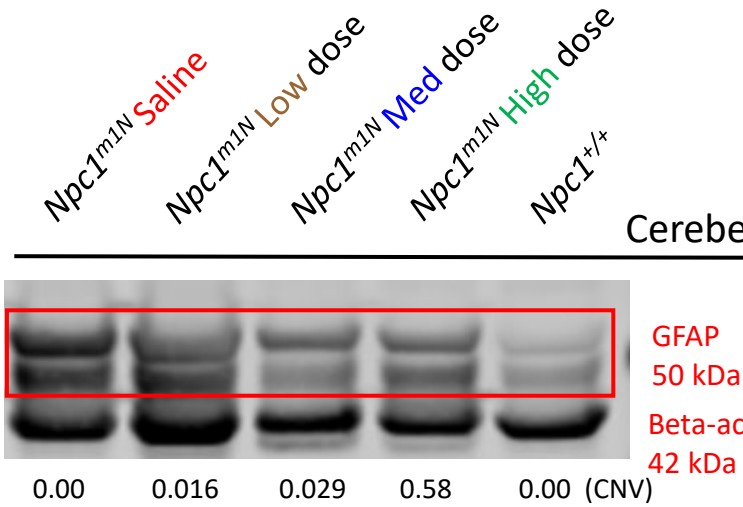

B

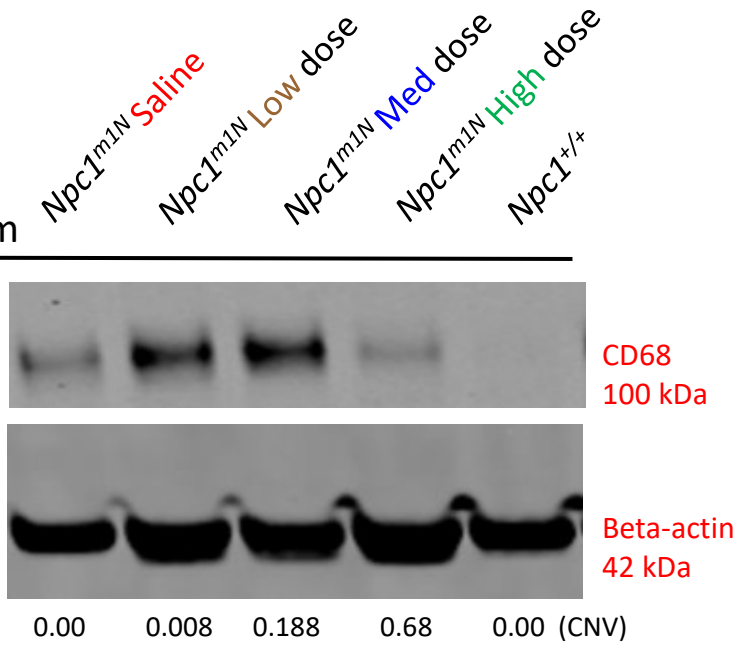

Figure S7. Representative blot for GFAP quantification (Fig 3C) and CD68 quantification (Fig 3E) in the cerebellum. *hNPC1* copy number variation listed under blot for each sample.

C

Original source data (GFAP, beta-actin; right half of blot enlarged).

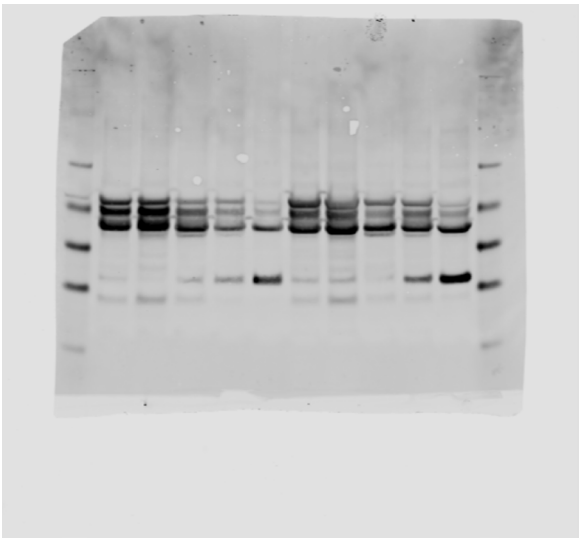

D

Original source data (CD68, beta-actin; left half of blot enlarged).

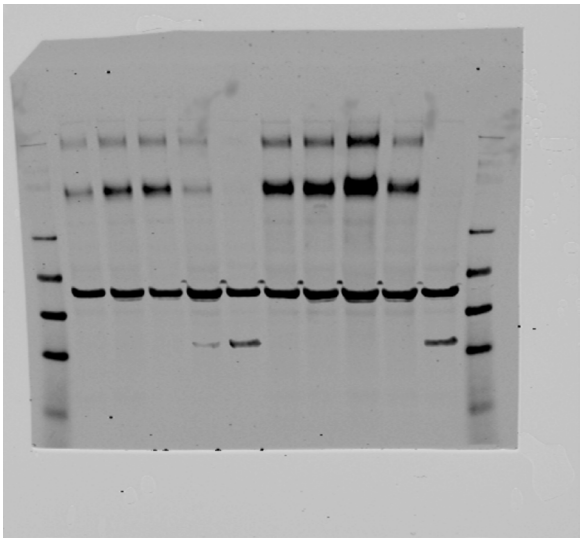

A

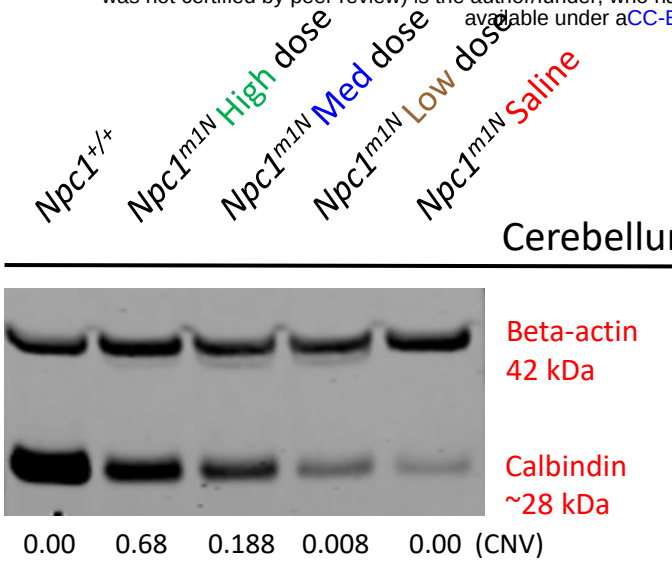

B

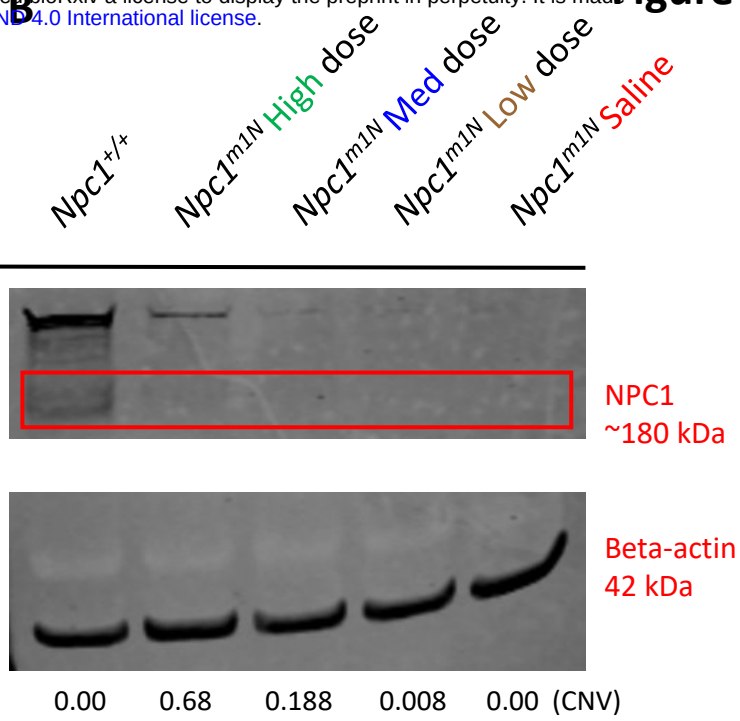

Figure S8. Representative blot for calbindin D quantification (Fig 3D) and NPC1 quantification (Fig 3G) in the cerebellum. *hNPC1* copy number variation listed under blot for each sample.

C

Original source data (Calbindin, beta-actin on right, NPC1, beta-actin on left).

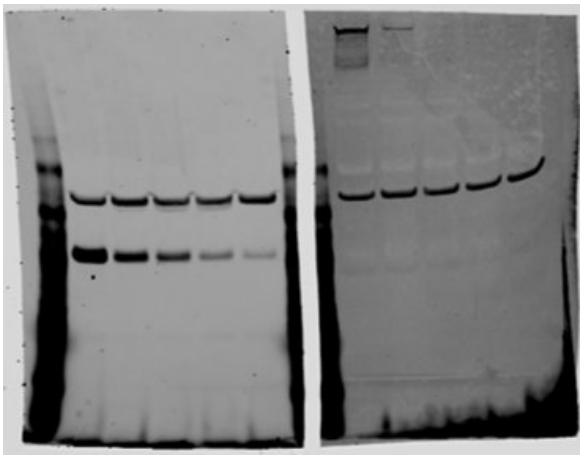

Figure S8